



Contrasting Air Pollution Responses to Hourly Varying Anthropogenic NO_x Emissions in the Contiguous United States

Madankui Tao^{1,2,3*,} Arlene M. Fiore^{1,2}, Louisa K. Emmons⁴, Jeffery R. Scott¹, Gabriele G. Pfister⁴, Duseong S. Jo⁵, Wenfu Tang⁴

- ¹Earth Atmospheric and Planetary Sciences, Massachusetts Institute of Technology, Cambridge, MA, 02139, USA,
 - ²Lamont-Doherty Earth Observatory, Columbia University, Palisades, NY, 10964, USA,
 - ³Department of Earth and Environmental Sciences, Columbia University, New York, NY, 10027, USA,
 - ⁴Atmospheric Chemistry Observations & Modeling Laboratory, National Center for Atmospheric Research, Boulder, CO, 80301, USA,
- 10 ⁵Department of Earth Science Education, Seoul National University, Gwanak-gu, Seoul, 08826, South Korea.

Correspondence to: Madankui Tao (taoma528@mit.edu)

Abstract (250 Word Limit)

Monthly mean concentrations of air pollutants such as tropospheric nitrogen dioxide (NO₂) columns retrieved from satellite instruments are frequently used to infer NO_x emissions. An underlying assumption, also implicit in some global models, is that hourly variations in emissions average out in monthly means. To characterize the impacts of hourly emission variations, we use a global model with a refined ~14 km resolution over the contiguous United States (CONUS; MUSICAv0) and a regional CONUS inventory for July 2018. Switching from daily to hourly nitric oxide (NO) emissions (typically higher during the day and lower at night) yields differing spatial responses in surface nitrogen oxides (NO_x \equiv NO+NO₂) and ozone (O₃) concentrations in western versus eastern CONUS and in urban versus rural areas. Neglecting hourly variations in CONUS NO emissions products leads to pixel-level monthly mean errors of -49 % to +86 % (-1 to +8 ppb) for surface NO₂ and -22 % to +11 % (-7 to +5 ppb) for O₃, with tropospheric NO₂ columns showing similar spatial patterns (-12 % to +56 %). Although comparable in magnitude to a uniform 30 % NO emission reduction (-12 % to +9 %, -7 to +3 ppb for O₃), these distinct spatial patterns in the concentration responses reflect the influence of location-specific emission timing and meteorology. We conclude that models used to infer NO_x emissions from monthly mean concentrations may alias hourly emission variations into the inferred magnitude of emitted NO.

1 Introduction

Exposure to ground-level ozone (O_3) pollution can intensify the risk of respiratory and cardiovascular diseases (Dedoussi et al., 2020; Di et al., 2017a, b; Strosnider et al., 2019). However, understanding the drivers of surface O_3 variations is challenging due to its formation through nonlinear photochemical reactions involving its precursors: nitrogen oxides (NO_x) , volatile organic compounds (VOCs), and carbon monoxide (CO). Nonlinear O_3 production sensitivity to NO_x and VOCs is



35

45

50

55



commonly described in terms of three photochemical regimes: the NO_x-saturated regime, in which O₃ concentrations increase with reductions in NO_x or increases in VOCs; the NO_x-sensitive regime, in which O₃ increases with increasing NO_x but shows limited response to VOCs; and a transitional regime, where O₃ responds similarly to changes in both precursors (Kleinman, 1994, 2005; Sillman, 2003; Sillman and He, 2002; Tonnesen and Dennis, 2000). Identifying these regimes in time and space requires diagnostic tools, and air quality models serve this role by bridging observational gaps, attributing pollution sources, and quantifying O₃ sensitivity to precursor emissions. Accurate anthropogenic emissions are critical for ensuring reliable model performance in these applications. We focus here on how temporal changes in emissions influence pollutant concentrations, highlighting the importance of accounting for diurnal variability when interpreting or inferring emissions from observed concentrations, and vice versa. Below, we specifically address the question: How does the temporal resolution (hourly, daily, or monthly) of anthropogenic emissions inventories affect model simulations of O₃ concentrations and its precursors, along with their spatiotemporal variations across the contiguous United States (CONUS)?

Recent advances in global chemistry models include the introduction of variable resolution options for continental-scale air pollution modeling (e.g., Wang et al., 2004; Goto et al., 2020; Krol et al., 2005), with studies showing that higher horizontal resolutions generally improve model alignment with observations (e.g., Schwantes et al., 2022; Jo et al., 2023; Yu et al., 2016). The variable resolution option provides high resolution over specified regions while avoiding the need for boundary conditions required by regional models, enabling studies of local-to-global influences on regional air pollution within a framework of globally consistent dynamics, physics, and chemistry. Version 0 of the Multi-Scale Infrastructure for Chemistry and Aerosols (MUSICAv0) is a configuration of the Community Atmosphere Model with chemistry (CAM-chem) and horizontal regional mesh refinement using the spectral element dynamical core (Pfister et al., 2020). Previous applications of MUSICAv0 have been used to investigate O₃ photochemistry in the southeast U.S. (Schwantes et al., 2022), the effects of wildfires (Tang et al., 2022, 2023b, 2025), and air quality in Africa (Tang et al., 2023a) and South Korea (Jo et al., 2023).

Global atmospheric chemistry models often do not represent daily and diurnal variations in anthropogenic emissions, instead using monthly averaged inventories, as high-temporal-resolution inventories are not always available for all regions, require substantial storage, and their influence on simulation results is uncertain and may, in some cases, be minimal. Options exist to incorporate diurnal and day-of-week variations directly in the input emissions files by providing all dates and hours, as we implement below, or by applying geographically varying scaling factors for selected regions and species (Keller et al., 2014; Lin et al., 2021). Jo et al. (2023) demonstrate that applying country-specific prescribed hourly diurnal profiles to monthly mean emissions over South Korea produces simulations that align better with observations of secondary species with strong diurnal variations like O₃ and NO_x, although they neglect day-to-day variability. Including sub-monthly temporal resolution for anthropogenic emissions increases the size of input files but has limited computational cost. Over our study domain (CONUS, defined in Fig. 1), we show below that neglecting these variations for NO emissions can lead to discrepancies in simulated monthly mean NO_x and O₃ concentrations, ranging from -49% to +86% for NO₂ concentrations and from -22% to +11% for O₃. These discrepancies are sufficiently large as to matter for informing air management efforts and imply potential for errors in model applications inferring emissions from satellite-based observations with once-daily overpasses.



70

90



We select July 2018 due to the availability of trace gas retrievals from the TROPOspheric Monitoring Instrument (TROPOMI) and concurrent field campaign observations, with our previous analyses indicating that much of New York City was in a transitional O₃ production regime but shifted toward more NO_x-sensitive conditions on the highest O₃ days, while the urban core may remain NO_x-saturated (Tao et al., 2022, 2025). We build from those insights to evaluate MUSICAv0 model simulations and examine diurnal variations in emissions and concentrations in this study. Section 2 describes our model framework and simulation design, including the BASE simulation using global anthropogenic emissions from CAMS-GLOB-ANT v5.1 and modifications introducing the adjusted 2017 U.S. National Emissions Inventory (NEI) over the CONUS (Section 2.1). Section 3 compares the model simulations against surface measurements of trace gases (O₃, NO₂, CO, and sulfur dioxide (SO₂)) and fine particulate matter (PM_{2.5}), as well as satellite retrievals of NO₂, HCHO, and CO from TROPOMI. After briefly describing these observational datasets (Section 3.1), we assess the impact of using NEI (Section 3.2) and incorporating hourly emission variations (Section 3.3) and examine diurnal and weekday-weekend patterns in pollutant concentrations (Section 3.4). Section 4 isolates the effects of resolving hourly nitric oxide (NO) emissions, first by examining west-to-east contrasts in surface pollutant responses (Section 4.1), and then through urban case studies in Los Angeles and New York City (Section 4.2). Section 5 summarizes the key findings and discusses their implications.

80 2 Model Description and Simulations

We use a standard configuration of MUSICAv0 that features a \sim 14 km \times 14 km refined grid for the CONUS ("ne0CONUSne30x8"), which has been shown to better represent observed surface concentrations of O_3 and its precursors such as NO_x and CO compared to the \sim 100 km ("ne30") global horizontal resolution (Schwantes et al., 2022). We conduct all simulations for the year 2018. The MUSICAv0 atmospheric model is a configuration of CAM6-chem, version 6 of the Community Atmosphere Model (CAM6), which is a component of the Community Earth System Model (CESM) version 2.2 (Danabasoglu et al., 2020; Emmons et al., 2020). The CAM meteorology is nudged to the 3-hourly Modern-Era Retrospective analysis for Research and Applications Version 2 (MERRA2) meteorology (Gelaro et al., 2017). The MUSICAv0 (CESM/CAM6-chem) model simulations use 32 vertical layers from the surface up to about 1 hPa (\sim 45 km) (Tilmes et al., 2019).

In the standard simulation (hereafter, BASE), we use MOZART-TS1 troposphere-stratosphere chemistry (Emmons et al., 2020; Tilmes et al., 2019), with monthly Copernicus Atmosphere Monitoring Service (CAMS-GLOB-ANT) v5.1 for global anthropogenic emissions (Eskes et al., 2021) and daily Fire Inventory from NCAR (National Center for Atmospheric Research) (FINN) v2.5 (Wiedinmyer et al., 2023) for biomass burning emissions. Biogenic emissions of VOCs and CO are calculated online in the land component of CESM (Lawrence et al., 2019) based on the Model of Emissions of Gases and Aerosols from Nature (MEGAN) version 2.1 (Guenther et al., 2012). Additional emissions, such as soil NO_x, oceanic CO, and hydrocarbons, are taken from the POET inventory (Granier et al., 2005). Dry deposition is calculated interactively through coupled atmospheric and land models, parameterized by meteorology and biophysics (Emmons et al., 2020). We prescribe





latitudinally varying fixed mixing ratio lower boundary conditions for carbon dioxide (CO₂), methane (CH₄), nitrous oxide (N₂O), and other well-mixed greenhouse gases, based on the ScenarioMIP SSP5-8.5 pathway from the Coupled Model Intercomparison Project Phase 6 (CMIP6) (Meinshausen et al., 2017; Montzka et al., 2004).

The BASE simulation covers the period from January to September 2018. The default nudging strength for CESM is 50 hours on 32 vertical levels. Previous studies using CESM2.2 have employed nudging relaxation times of 50 hours (Schwantes et al., 2020), 12 hours (Tang et al., 2023b), and 6 hours (Tang et al., 2022). For the BASE simulation, we adopt an intermediate option of 12-hour nudging relaxation time as recommended for driving the model with 3-hour meteorology fields (Davis et al., 2022; Gaubert et al., 2020; Schwantes et al., 2022). Only 'T' (air temperature), 'U' (zonal wind velocity), and 'V' (meridional wind velocity) are nudged. We conduct short perturbation simulations relative to the BASE case from July 1-5, 2018 (Table S1) to test sensitivity to changes in total anthropogenic and biogenic emissions and to an alternative chemical mechanism with more detailed isoprene and terpene chemistry (Schwantes et al., 2022), providing context for interpreting the BASE case and confirming that our model setup responds consistently with previous studies (Text S1; Figs. S1 and S2). We also confirm that using 12-hour nudging maintains consistent meteorological conditions (T, U, V) across scenarios, ensuring that weather variability does not substantially affect conclusions drawn by differencing simulations (Text S2; Fig. S3). For simulations covering July 2018 (Table 1), we save hourly mean diagnostics of meteorological conditions, concentrations of major trace gases and aerosols, their deposition fluxes, as well as O₃ production and loss rates.

115

100

105



120

130

135



Table 1: MUSICAv0 BASE configuration (January-September 2018) and NEI sensitivity simulations with modifications (Section 2.1) to anthropogenic emissions (July 2018).

Simulation ID	Emissions Perturbation
BASE	No
NEI_monthly	Monthly NEI data replaces the CAMS-GLOB-ANT v5.1 anthropogenic emissions over the CONUS
NEI_monthly_m30anthroNO	Same as NEI_monthly, but anthropogenic NO emissions are reduced by 30%
NEI_monthly_m30anthroVOC	Same as NEI_monthly, but anthropogenic VOC emissions are reduced by 30%
NEI_hourly	Hourly NEI data replaces anthropogenic emissions over the CONUS
NEI_hourly_NO	Same as NEI_monthly, but with hourly NO emissions from the NEI over the CONUS
NEI_daily_NO	Same as NEI_monthly, but with daily-mean NO emissions from the NEI over the CONUS

2.1 Modifications to the CONUS Anthropogenic Emissions Inventory

CAMS-GLOB-ANT provides monthly averages for 36 emitted compounds within 17 sectors at a spatial resolution of $0.1^{\circ} \times 0.1^{\circ}$ (latitude × longitude) (Soulie et al., 2023). Here, we use CAMS-GLOB-ANT version 5.1 (Eskes et al., 2021), which combines the Emissions Database for Global Atmospheric Research (EDGAR) v5 (Crippa et al., 2019) up to 2015 with the Community Emissions Data System (CEDS) (McDuffie et al., 2020) to extrapolate emissions from 2016 to 2021.

The U.S. Environmental Protection Agency (EPA) National Emissions Inventory (NEI) is a national inventory that includes emissions of criteria pollutants, precursors, and hazardous air pollutants (U.S. Environmental Protection Agency, 2024). The NEI is updated every three years and constructed through the Emissions Inventory System (EIS), which collects and integrates data primarily provided by State, Local, and Tribal air agencies. We start from the 2017 NEI (U.S. Environmental Protection Agency, 2022), processed to hourly resolution on a ~0.1° × 0.1° grid over the CONUS (Supplemental Text S3) using sector-specific diurnal profiles to capture within-day as well as day-to-day variations. The hourly NEI data are first shifted to match the 2018 weekday/weekend calendar, then re-gridded (mass-conserving) to the unstructured ne0CONUSne30x8 horizontal resolution using NCAR-developed tools (National Center for Atmospheric Research, 2022a, b), and averaged to daily or monthly means. We replace CAMS-GLOB-ANT v5.1 emissions over the CONUS with these NEI products (hourly, daily, or monthly), retaining CAMS monthly means elsewhere. The NEI products capture weekday/weekend differences in hourly and daily forms but not in monthly means.

Switching to NEI from CAMS-GLOB-ANT v5.1 emissions yields widespread decreases in most emitted species, particularly monthly mean NO and CO emissions (Fig. S4). Changes in anthropogenic VOC emissions are negligible since biogenic emissions are much higher than anthropogenic emissions (compare Fig. S5 to Fig. S4). A comprehensive list of emitted VOC species is provided in Text S4.



140

145

150

165



To assess the impact of using an alternate anthropogenic emissions inventory and different temporal resolutions of emissions, we conduct four one-month simulations (Table 1): 1) monthly NEI data replace CAMS-GLOB-ANT v5.1 emissions over the CONUS, with CAMS monthly means retained elsewhere (NEI_monthly); 2) as in NEI_monthly except for hourly NEI emissions for all species over the CONUS (NEI_hourly); 3) as in NEI_monthly, but applying hourly variability only to NO emissions (NEI_hourly_NO); 4) as in NEI_monthly, but applying daily NO emissions with weekday-weekend differences (NEI_daily_NO). The NEI_monthly vs. BASE comparison isolates the effect of changing emission inventories, NEI_hourly vs. NEI_monthly assesses the influence of adding sub-monthly and diurnal variability for all anthropogenic emissions, NEI_daily_NO vs. NEI_monthly isolates the effect of weekday-weekend differences in NO emissions, and NEI_hourly_NO vs. NEI_daily_NO isolates the effect of the diurnal changes in NO emission.

We conduct two additional one-month simulations using the NEI_monthly case as the reference to analyze the O₃ production regime under perturbations to anthropogenic NO_x and VOC emissions. In one simulation, we reduce anthropogenic NO emissions by 30% (NEI_monthly_m30anthroNO) and in another we reduce anthropogenic VOC emissions by 30% (NEI_monthly_m30anthroVOC) (Table 1). These additional sensitivity simulations provide context for those incorporating the more nuanced changes in the temporal resolution of anthropogenic emissions (Text S4).

3 Evaluating the Sensitivity of Simulated Air Pollution to Emission Inventory Choice and Temporal Resolution

To account for regional variation, we divide the CONUS into six regions: West Coast, Mountain, Midwest, Southwest, Northeast, and Southeast (Fig. 1). For each region, Fig. 2 compares modeled (Section 2) and observed (Section 3.1) July mean surface concentrations of NO₂, O₃, and CO, as well as VCDs of NO₂, HCHO, and CO. We evaluate the model spatial representation of the observations using Spearman's rank correlation coefficient (r_s) and mean bias error (MBE), calculated from monthly mean values at all grid cells within the selected domain. Detailed statistics for July mean values, including root mean square error (RMSE) as well as absolute and relative differences for both MBE and RMSE, are provided in Table S2.

Our primary focus is on O₃ and its precursors, though we include evaluations of surface SO₂ and PM_{2.5} in Supplement Text S5, Fig. S2, and Table S3.

3.1 Observational Datasets for Model Evaluation

We use measurements collected from State and Local Air Monitoring Stations (SLAMS) that are reported to the U.S. EPA Air Quality System (AQS) for trace gases (O₃, NO₂, CO, and SO₂) and PM_{2.5} concentrations (Table S4), downloaded from the AQS AirData portal (https://aqs.epa.gov/aqsweb/airdata/download_files.html; accessed August 2023). To compare MUSICAv0 surface simulations with SLAMS surface measurements, we identify the closest model grid cell based on the latitude and longitude of the SLAMS monitors. We then align hourly concentrations in local time from SLAMS with MUSICAv0 for each species across all CONUS monitors. A limitation of this evaluation is that most SLAMS sites are in urban



170

175

180

185

190

200



areas and are influenced by localized effects that cannot be fully resolved by the model at 14 km resolution, which may affect the representativeness of site-level comparisons.

We select six monitoring stations as examples to examine diurnal patterns at individual sites (Table S5). These representative urban sites were chosen based on their proximity to major city centers across the CONUS and the availability of continuous NO₂ and O₃ measurements throughout July 2018. Nearby stations with similar diurnal behavior were excluded to avoid redundancy, and averaging across sites was avoided to preserve distinct local features given differences in monitor availability across cities.

We also use retrievals from TROPOMI, a nadir-viewing shortwave spectrometer aboard the Sentinel 5 Precursor (S5P) satellite launched in 2017 and operational in 2018. We compare tropospheric vertical column densities (VCD_{Trop}) of NO₂ (5.5 km × 3.5 km) and HCHO (5.5 km × 3.5 km), along with total vertical column densities (VCD_{Total}) of CO (5.5 km × 7 km) retrieved from TROPOMI, using products (RPRO Version 02.04.00; accessed December 2023) selected for pixels with quality assurance greater than 0.75 (Table S4). We re-grid the column densities and corresponding averaging kernels (AKs) to a horizontal resolution of 0.15° × 0.15°, slightly coarser than that of the model simulations over the CONUS (approximately 0.125°). TROPOMI uses *a priori* profiles derived from the TM5-MP global chemistry transport model (Myriokefalitakis et al., 2020), the massively parallel (MP) version of the Tracer Model version 5 (TM5), to simulate the vertical distribution of NO₂, HCHO, and CO, which are provided as supplementary data with the Level-2 products. The TM5-MP model provides data at a 1° × 1° horizontal resolution for the troposphere and upper troposphere-lower stratosphere on 34 hybrid sigma-pressure levels from the surface to approximately 0.1 hPa for retrieving the VCD_{trop} of NO₂ and HCHO (Williams et al., 2017). The CO total column density retrievals are based on 50 hybrid sigma-pressure levels from TM5-MP.

To compare modeled column densities with TROPOMI retrievals, we mass conservatively re-grid the hourly MUSICAv0 HCHO, NO₂, CO, and meteorological variables to a 0.15° × 0.15° finite volume grid. We calculate the average between 1 and 2 p.m. local time (to approximate 1:30 p.m. values) for each region and apply the TROPOMI AKs, linearly interpolated vertically to the MUSICAv0 vertical resolution, to calculate modeled VCD_{Trop} of NO₂ and HCHO and VCD_{Total} of CO. We use the tropopause height diagnosed from the model simulations. Applying AKs to the modeled column enables a more consistent comparison between model simulations and satellite retrievals by accounting for the vertical sensitivity of the satellite instrument. We compare daily 1:30 p.m. VCD_{trop} or VCD_{Total} values across individual grid cells, matching each valid retrieval to the nearest model grid cell. Reported averages include only grid cells with valid retrievals.

3.2 Choice of Monthly Emission Inventory (BASE vs. NEI_monthly) Influences Simulated Air Pollution

Because model performance varies substantially across regions, we focus on region-specific comparisons with observations across the CONUS, as national-level summaries may obscure important regional differences. Across the six CONUS regions, spatial correlations between modeled and observed surface concentrations are stronger for NO₂ and O₃ (r_s typically > 0.5) than for CO (r_s = 0.10-0.36) (Fig. 2). Modeled surface concentrations of NO₂ are biased high by 22-40% (2-5 ppb) in all regions except the Mountain region, which shows an average low bias of 18% (1 ppb). Modeled July mean surface



205

210

215

220

225

230



O₃ concentrations are overestimated by 11-29% (6-13 ppb). Surface CO is underestimated by 17-87% (27-140 ppb) compared to SLAMS across all regions. Modeled July mean VCDs correlate spatially with TROPOMI NO₂ VCD_{Trop} (r_s : 0.65-0.85) and HCHO VCD_{Trop} (r_s = 0.60-0.92), though the correlation is weak for CO VCD_{Total} (r_s = 0.11-0.53). Modeled NO₂ VCD_{Trop} is underestimated by 34-48% (~3×10¹⁴ molecules/cm²), while HCHO VCD_{Trop} is overestimated by 15-24% (1-4×10¹⁵ molecules/cm²) across the six regions. CO VCD_{Total} is underestimated by 2-11% (3-18×10¹⁶ molecules/cm²) in the West Coast, Midwest, and Northeast, but overestimated by 2-8% (3-14×10¹⁶ molecules/cm²) in the Mountain, Southwest, and Southeast regions.

Compared to the BASE case, NEI_monthly (which uses monthly NEI emissions over the CONUS) improves spatial correlations (r_s) and reduces model biases (MBE and RMSE) for surface NO₂, CO, and O₃ concentrations, particularly in the Northeast region (Fig. 2). Differences in simulated surface NO₂ and CO between NEI_monthly and BASE (Fig. 2) reflect emissions changes in NO and CO due to the shift from CAMS-GLOB-ANT v5.1 to NEI (Fig. S4), showing heterogeneous spatial patterns but generally NO reductions and CO increases, particularly over the eastern CONUS and some urban centers. Lower NEI NO emissions (Fig. S4c) reduce regional mean NO₂ concentrations by 1-6 ppb, bringing high biases down to within 1 ppb but exacerbating the low bias in the Mountain region to -2 ppb (Fig. 2). CO concentrations increase relative to the BASE simulation, thus improving surface CO underestimation by 13-55% (20-65 ppb), although low biases of 1-33% (2-71 ppb) remain (Fig. 2). For secondary pollutants like O₃, changes in concentrations do not directly mirror emissions perturbations. Compared to the BASE case, surface O₃ concentrations decrease in NEI_monthly, except in cities with higher NO_x emissions, thereby reducing modeled surface O₃ biases relative to SLAMS by 2-11% (approximately 1-6 ppb) across the six regional means. However, model biases of 3-21% (1-8 ppb) remain across all regions, particularly on the West Coast.

There are minimal to no changes in r_s for HCHO VCD_{Trop}, while NO₂ VCD_{Trop} shows weaker correlations and worsening model biases, and changes in CO VCD_{Total} exhibit large regional variability. Switching to NEI consistently decreases both surface and column NO₂ but not CO (Fig. 2). Compared to the BASE case, the NEI_monthly simulation worsens the model underestimates of NO₂ VCD_{Trop} by 16-21% (\sim 1×10¹⁴ molecules/cm²) but decreases overestimates of regional mean HCHO VCD_{Trop} by approximately 2% (0.2-4×10¹⁴ molecules/cm²) across all regions. CO VCD_{Total} shows slight increases (less than 1%) in the Southeast and slight decreases (under 2%) in other regions, with the sign of the model bias unchanged from the BASE simulation. Biases in trace gas columns do not always match those at the surface. For instance, surface NO₂ shows slight high biases in some regions, while column NO₂ generally has a low bias relative to TROPOMI. These discrepancies reflect vertical distribution heterogeneity and diurnal variation, as column comparisons are for 1:30 p.m. local time, while surface comparisons include all times of the day.

3.3 Incorporating Hourly Variations in Emissions (NEI hourly) Affects Monthly Mean Pollutant Concentrations

The surface NO₂ and O₃ concentration changes between NEI_hourly and NEI_monthly are, in some regions, similar in magnitude to those between NEI_monthly_m30anthroNO (a 30% reduction in anthropogenic NO emissions) and NEI monthly, but the spatial patterns in differences differ markedly (Fig. 3a). These differences between NEI_hourly and



250



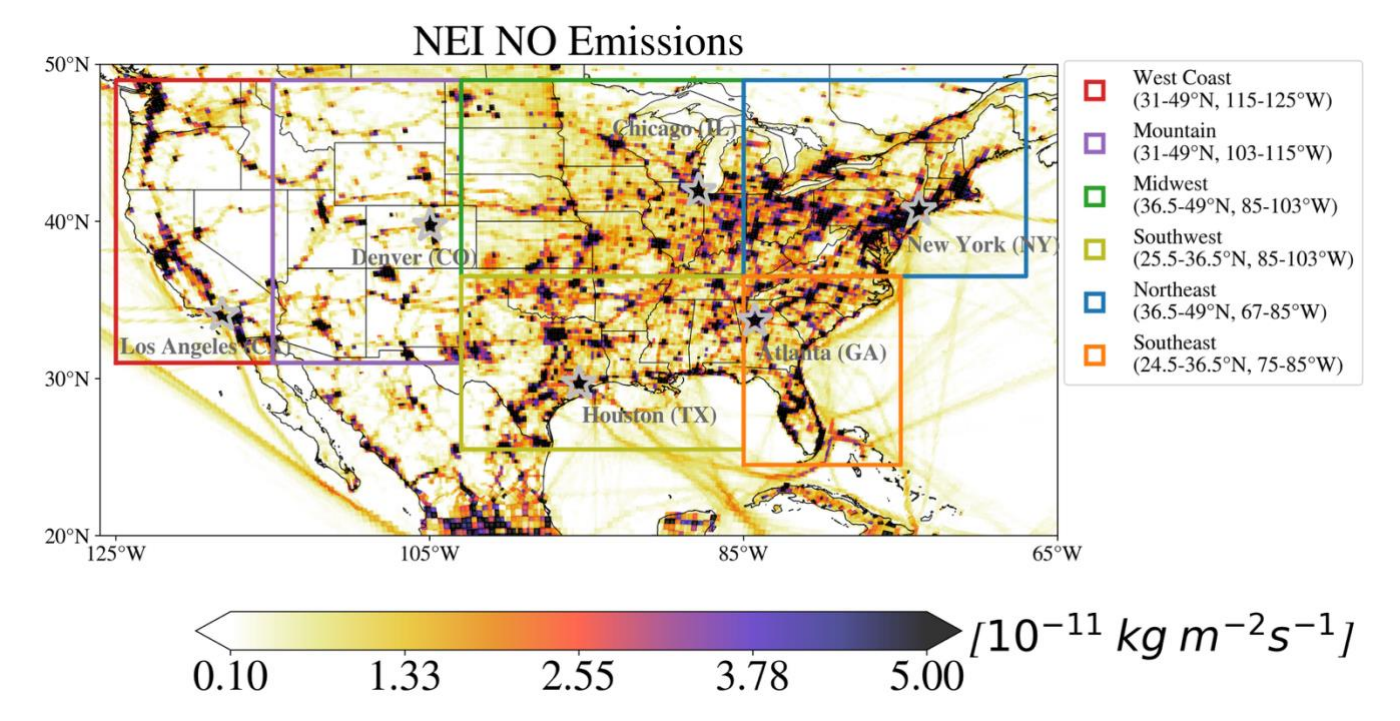
NEI_monthly reflect temporal redistribution of emissions rather than changes in their total amounts. Although overall agreement with observations changes only slightly (*r_s*, MBE, and RMSE; Fig. 2 and Table S1), the direction and magnitude of concentration changes vary substantially across regions, especially between urban and rural areas and between the western and eastern CONUS.

The largest July regional-mean difference in surface NO₂ (NEI_hourly – NEI_monthly) occurs on the West Coast (+16%, or +0.3 ppb), while the largest decrease is in the Northeast (-7%, -0.1 ppb) (Fig. 3). As a result, the model shifts from underestimation to overestimation on the West Coast, while the underestimation in the Northeast becomes more pronounced for surface NO₂ when compared with SLAMS observations (Fig. 2). For surface CO, changes are small and spatially varied, with regional mean increases of 2-7% (4-10 ppb) in the West Coast, Mountain, Midwest, and Southwest, and decreases of about 3% (~5 ppb) in the Northeast and Southeast (Fig. 3). For NEI_hourly – NEI_monthly, changes in NO₂ VCD_{Trop} and CO VCD_{Total} largely mirror the surface patterns (Fig. 3b).

High model biases persist for surface O_3 concentrations (5-20%; 3-9 ppb) after incorporating hourly variations in emissions (Fig. 2). Monthly mean surface O_3 concentrations decrease by up to ~2% (<1 ppb) in the Midwest, Northeast, and Southeast, while increases of up to ~3% (1-4 ppb) in other regions slightly worsen model overestimation. Although surface HCHO observations are unavailable for evaluation, modeled changes remain under 3% and follow similar spatial patterns to those of surface O_3 (Fig. 3). Monthly mean HCHO VCD_{Trop} decreases in the Midwest, Northeast, and Southeast but increases in other regions, mirroring the regional pattern of surface HCHO changes (Fig. 3), despite a persistent high model bias of 14-23% (1-3×10¹⁵ molecules/cm²) (Fig. 2).





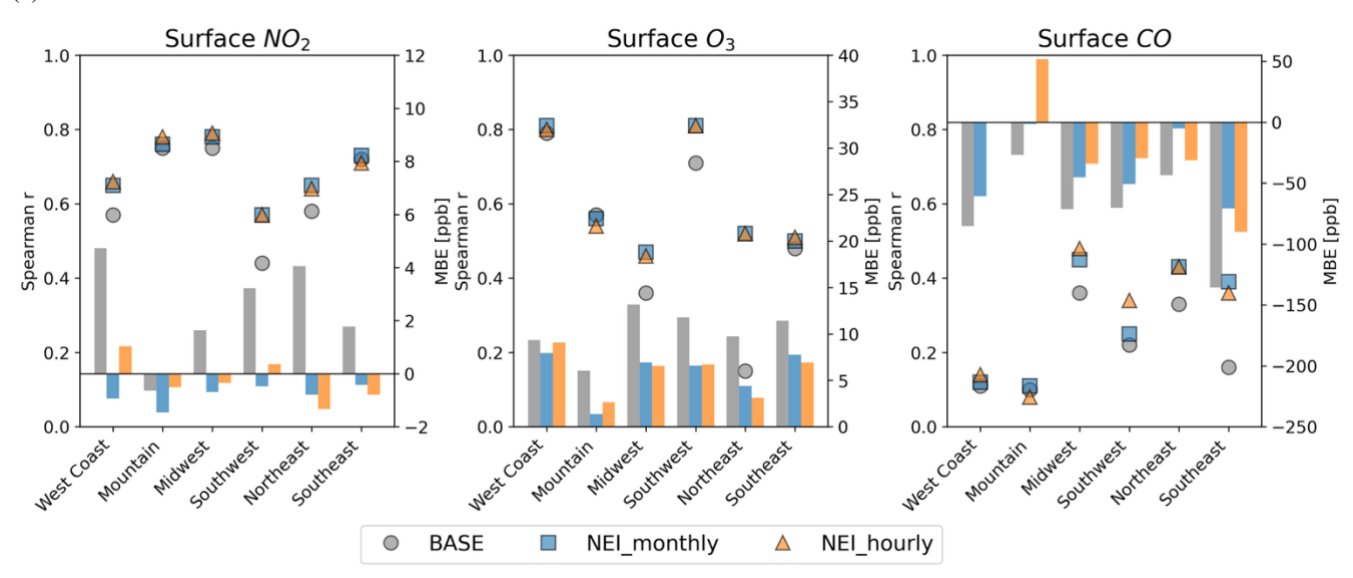


255 Fig. 1: July mean nitric oxide (NO) emissions from the adjusted 2017 National Emissions Inventory, divided into six regions for model analysis: West Coast (red), Mountain (purple), Midwest (green), Southwest (yellow), Northeast (blue), and Southeast (orange). The locations of selected State and Local Monitoring Stations (SLAMS) in six major cities—Los Angeles (CA), Chicago (IL), New York City (NY), Denver (CO), Houston (TX), and Atlanta (GA)—are marked with stars. The monitor site IDs and locations are listed in Table S5.





(a) Surface concentrations



(b) Tropospheric vertical column densities (VCD_{Trop})

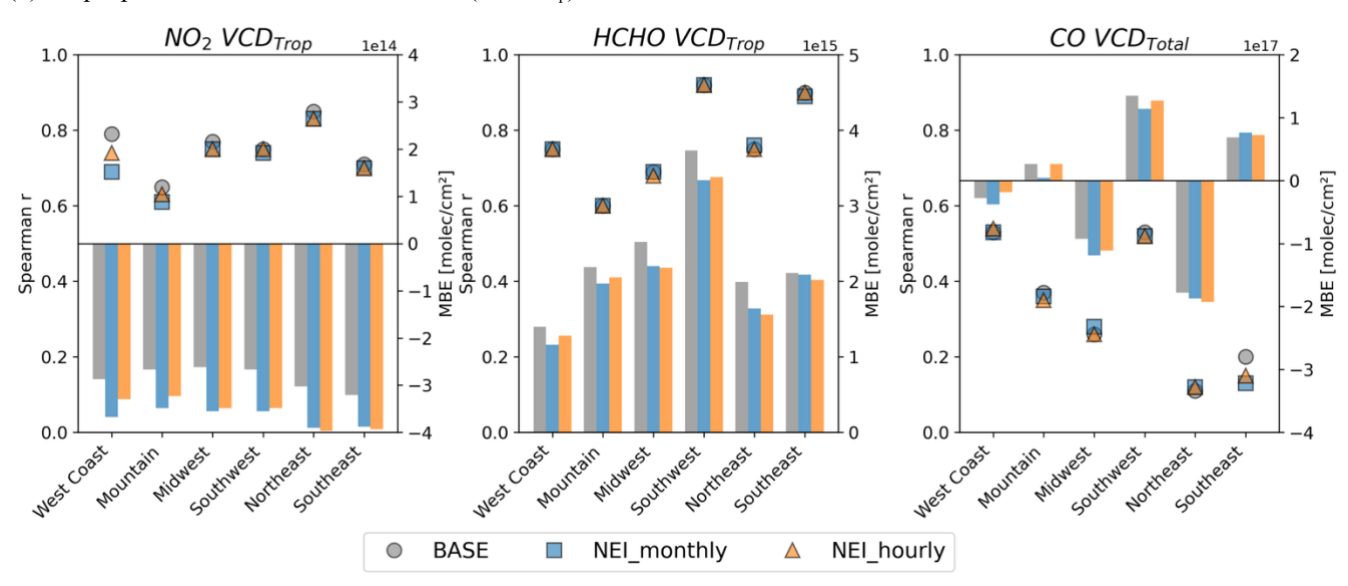
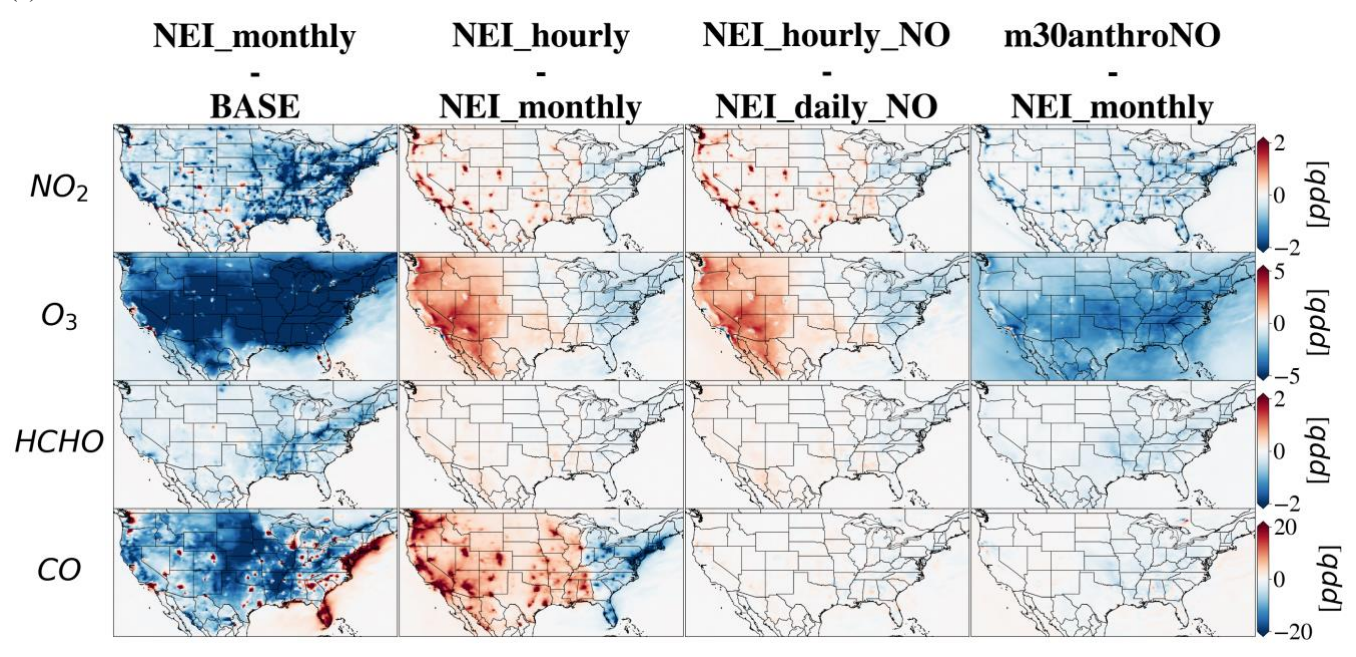


Fig. 2: Switching to monthly NEI emissions generally improves spatial correlations and reduces biases compared with observations, whereas changes in emissions temporal resolution have smaller effects; both impacts differ by region. Shown are MUSICAv0-simulated (a) surface concentrations of NO₂, O₃, and CO, and (b) column densities of NO₂, HCHO, and CO compared with observations (AQS for surface; TROPOMI for columns) for July 2018 across the six U.S. regions indicated in Fig. 1. Mean bias error (MBE; right axis) is shown as colored bars, and Spearman correlation coefficients (*r*₅; left axis) are shown as colored markers with distinct shapes. Scenarios are represented consistently: BASE (gray bars/circles), NEI_monthly (blue bars/squares), and NEI_hourly (orange bars/triangles). We provide detailed statistics in Table S2, including root mean square error (RMSE) and both absolute and relative differences for MBE and RMSE.





(a) Surface concentrations



(b) Tropospheric vertical column densities (VCD_{Trop})

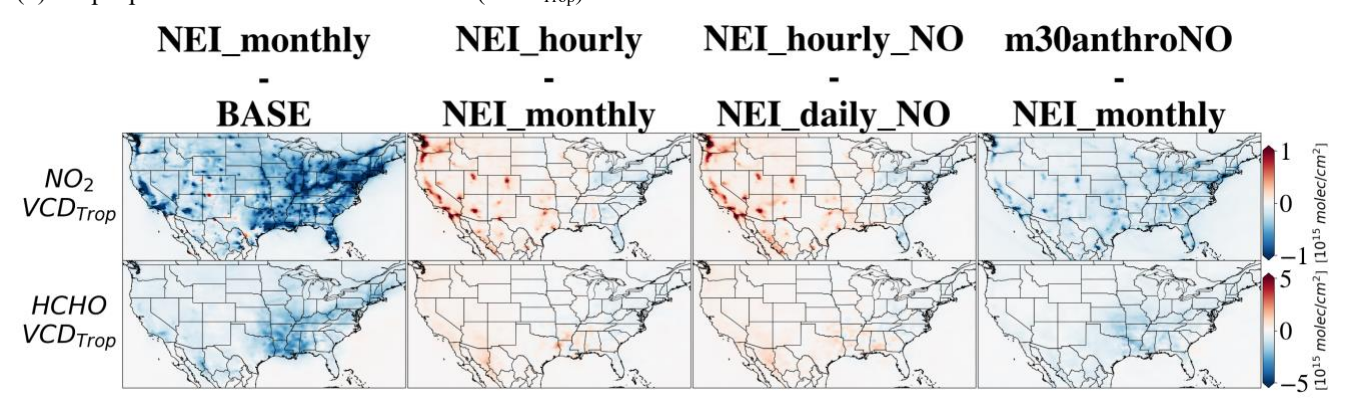


Fig. 3: Resolving hourly variations in NO emissions produces distinct spatial responses in surface concentrations, with absolute changes comparable to those from a uniform 30% reduction in monthly mean NO emissions; column changes generally mirror surface responses. Responses of selected trace gas species are shown (rows: surface concentrations in panel a, column densities in panel b) as differences in July monthly means (columns; see Table 1). Consistent color-bar ranges are used for each variable. See Fig. S3 for differences in surface SO₂ and PM_{2.5}. Fig. S8 provides comparisons of NEI_monthly with NEI_hourly_NO and NEI_daily_NO for completeness, as the main spatial differences in July mean surface concentrations are primarily driven by the addition of hourly variability in NO emissions (NEI_hourly_NO vs. NEI_daily_NO).

285

280







40 20

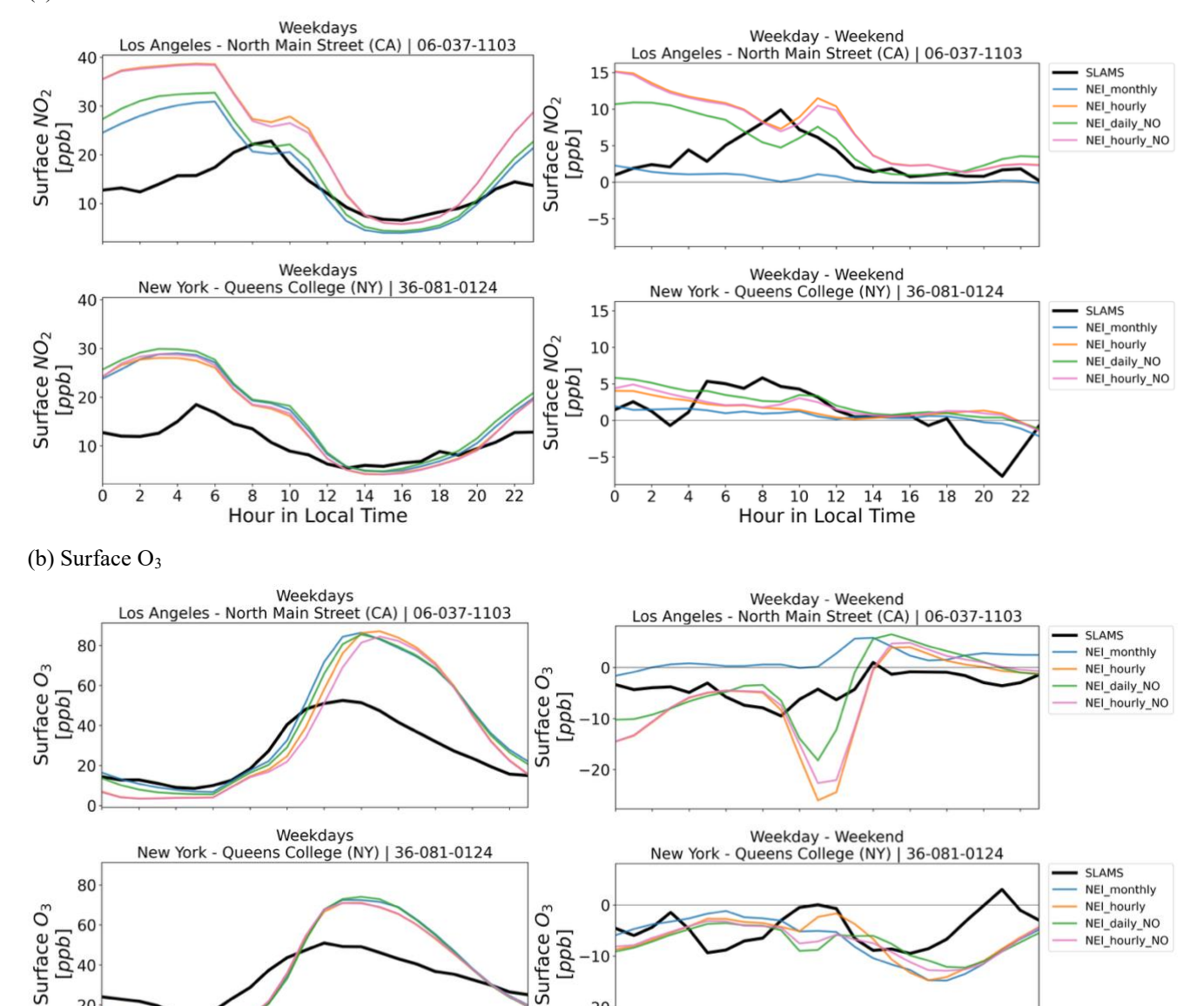
8

12

Hour in Local Time

14 16

18 20



290 Fig. 4: Our model simulations broadly capture diurnal and weekday-weekend variations in surface NO2 and O3, though they often exaggerate the daily range and weekday-weekend differences and may misrepresent peak timing. We show hourly variations in surface NO₂ (a) and O₃ (b) concentrations averaged for July 2018, for weekdays (left column) and weekday-minus-weekend differences (right column; horizontal gray line indicates zero change) at urban monitoring stations in Los Angeles (first row) and New York City (second row). Site names and IDs are shown in the figure titles, with locations in Table S5. Observations from SLAMS 295 are in black. Model simulations are shown in four scenarios: NEI monthly (blue), NEI hourly (orange), NEI daily NO (green), and NEI_hourly_NO (pink) (Table 1). Near-surface simulations are approximated at the nearest pixel to each monitoring station. Chicago, Denver, Houston, and Atlanta (Fig. 1) are shown in Fig. S7.

-20

Ó

8 10 12 14 16

Hour in Local Time



300

305

310

315

320



3.4 Model Evaluation: Diurnal Variability and Weekday-Weekend Differences

Our model simulations (Table 1) broadly capture day-to-day variations in surface NO₂ and O₃ at the six urban sites (Fig. S6), but they tend to overestimate both the daily range and the weekday-weekend differences and misrepresent the timing of peak concentrations in most cities (Figs. 4 and S7). Fig. 4 illustrates this for Los Angeles and New York City, showing observed and modeled July mean hourly variations in surface NO₂ and O₃ concentrations for weekdays (left) and weekday-minus-weekend differences (right). Analysis for Denver, Chicago, Houston, and Atlanta is provided in Fig. S7.

The exaggerated daily range largely reflects opposite model biases at different times of day: the model overestimates nighttime NO₂ (when concentrations are highest) and underestimates O₃ (at their lowest levels), while at midday it underestimates NO₂ and overestimates O₃, thereby amplifying the diurnal amplitude relative to observations (Figs. 4 and S7). The model may also misrepresent the timing of daily peaks. In Los Angeles, the simulated NO₂ maximum occurs at 6 a.m., about two hours earlier than observed (Fig. 4). In New York City, the timing aligns more closely, but the model fails to capture the pre-sunrise accumulation of NO₂. For O₃, the modeled daily maximum lags observations by about two hours in both Los Angeles and New York City, peaking at 2 p.m. (modeled) instead of noon (observed) (Fig. 4). These results highlight the need for improved representation of diurnal cycles, particularly boundary-layer dynamics that strongly shape near-surface concentrations (Adams et al., 2023), as biases in daily range and peak timing increase uncertainty and limit the application of model simulations, particularly in the era of high-temporal-resolution observations from satellites and ground-based networks.

As expected, simulations with day-to-day variations in emissions better capture weekday-weekend concentration differences compared to NEI_monthly, though the diurnal shape still does not match observations (see the right column of Figs. 4 and S7). Among the six cities considered, the largest weekday-weekend differences in surface NO₂ occur in Los Angeles. We find non-zero weekday-weekend concentration differences in the NEI_monthly simulation (blue line in Fig. 4), despite no weekday-weekend emission cycle being applied. These differences likely arise from meteorological variability, with stronger effects on O₃ than for NO₂. While the model generally captures the magnitude of weekday-weekend differences with day-to-day emission variations, it misplaces the timing: simulated differences peak from midnight to noon, whereas observations peak between 4 a.m. and noon in most cities. The model also overestimates the observed weekend O₃ decreases between 10 a.m. and noon in both Los Angeles and New York City. This analysis points to the importance of accounting for weekday-weekend emission cycles in models, combined with accurate simulation of meteorological variations.

4 Sensitivity to Hourly Variations in Nitric Oxide Emissions

When we impose hourly-varying emissions, we find responses that vary in sign by region and even change the monthly mean surface concentrations of NO₂, HCHO, and O₃, indicating substantial sensitivity to the timing of the emission. In particular, note the contrasting changes over the western versus eastern CONUS, and between urban versus rural areas (Fig. 3). We further demonstrate that these simulated responses produced by switching from NEI-monthly to NEI_hourly are primarily driven by the hourly variations in NO emissions (Fig. 3), evidenced by minimal changes between NEI hourly NO



335

340

345

350

355

360



and NEI_hourly (<0.5% for NO₂, HCHO, and O₃). Comparisons between NEI_daily_NO and NEI_monthly, and between NEI_hourly_NO and NEI_daily_NO, indicate that these spatial patterns are shaped by switching from daily mean to hourly varying NO emissions (Figs. 3 and S8).

Across the CONUS, switching from daily mean to hourly NO emissions increases daytime and decreases nighttime emissions, with larger differences on weekdays, thereby influencing surface NO_x concentrations and secondary pollutants like O₃, as illustrated in Figs. 6 and 7. We first examine the broad west-to-east contrasts in pollutant responses to incorporating hourly NO emissions (Section 4.1), with Fig. 5 showing July daytime (9 a.m.-5 p.m. local time) changes across the CONUS. We then analyze two representative urban centers: Los Angeles (CA) and New York City (NY), to examine how differences in emission timing, boundary layer dynamics, and photochemistry shape site-specific responses (Section 4.2). West-East Contrasts in Surface Pollutant Responses

To understand the broader impacts of incorporating hourly NO emissions, we begin by examining regional contrasts in July daytime responses across the CONUS, as shown in Fig. 5. Panel (a) maps the differences in surface NO, NO₂, O₃, and HCHO concentrations (NEI_hourly_NO minus NEI_daily_NO), while panel (b) summarizes the meridional means in 5° longitudinal bins. These plots highlight a west-to-east gradient in pollutant responses driven solely by adding the diel cycle to NO emissions. To help interpret this spatial variability, panel (c) presents the corresponding NEI_daily_NO daytime emissions and key meteorological variables, including surface temperature, PBL height, relative humidity, and NO₂ lifetime against dry deposition.

Polluted regions with higher NO emissions show more pronounced NO_x concentration responses (compare Figs. 1 and 3). In the western CONUS, July daytime (9 a.m.-5 p.m.) monthly mean surface NO and NO₂ concentrations increase by up to 8 ppb and 6 ppb, respectively, in urban areas in NEI_hourly_NO simulation relative to NEI_daily_NO (Fig. 5a-b). In contrast, monthly mean daytime surface NO and NO₂ decrease over the eastern CONUS by up to ~1 ppb, respectively, with the largest changes also concentrated in urban areas. However, changes in surface O₃ do not always coincide with the largest NO_x concentration changes. In the eastern CONUS, O₃ decreases by up to ~2 ppb, with the largest reductions over urban centers, consistent with prior findings (e.g., Jo et al., 2023) highlighting the sensitivity of concentration changes to emission timing in polluted regions. In contrast, monthly mean O₃ increases of up to 8 ppb occur over the western CONUS along the edges of —not within— urban areas. This spatial pattern points to enhanced NO_x sensitivity at the periphery of NO_x-saturated western urban cores, consistent with our sensitivity simulations relative to the BASE case, where a 30% reduction in anthropogenic NO emissions yields the largest O₃ changes in surrounding rural areas (Fig. 3). In the West, the mean of the NEI_hourly_NO minus NEI_daily_NO differences exceeds the median, driven by large NO_x increases in a few urban grid cells. In the East, the lower mean relative to the median reflects strong but localized NO_x decreases. By contrast, O₃ differences show closer agreement between mean and median across both regions, suggesting more spatially uniform impacts (Fig. 5c). This spatial contrast occurs at nighttime (11 p.m.-5 a.m.) as well, with changes in the same direction as daytime (Fig. S9).

These spatial patterns are likely shaped by a complex interplay of background anthropogenic and biogenic emissions, local photochemical conditions, meteorology (especially boundary layer dynamics and transport), and deposition. In July, the



365

370

375

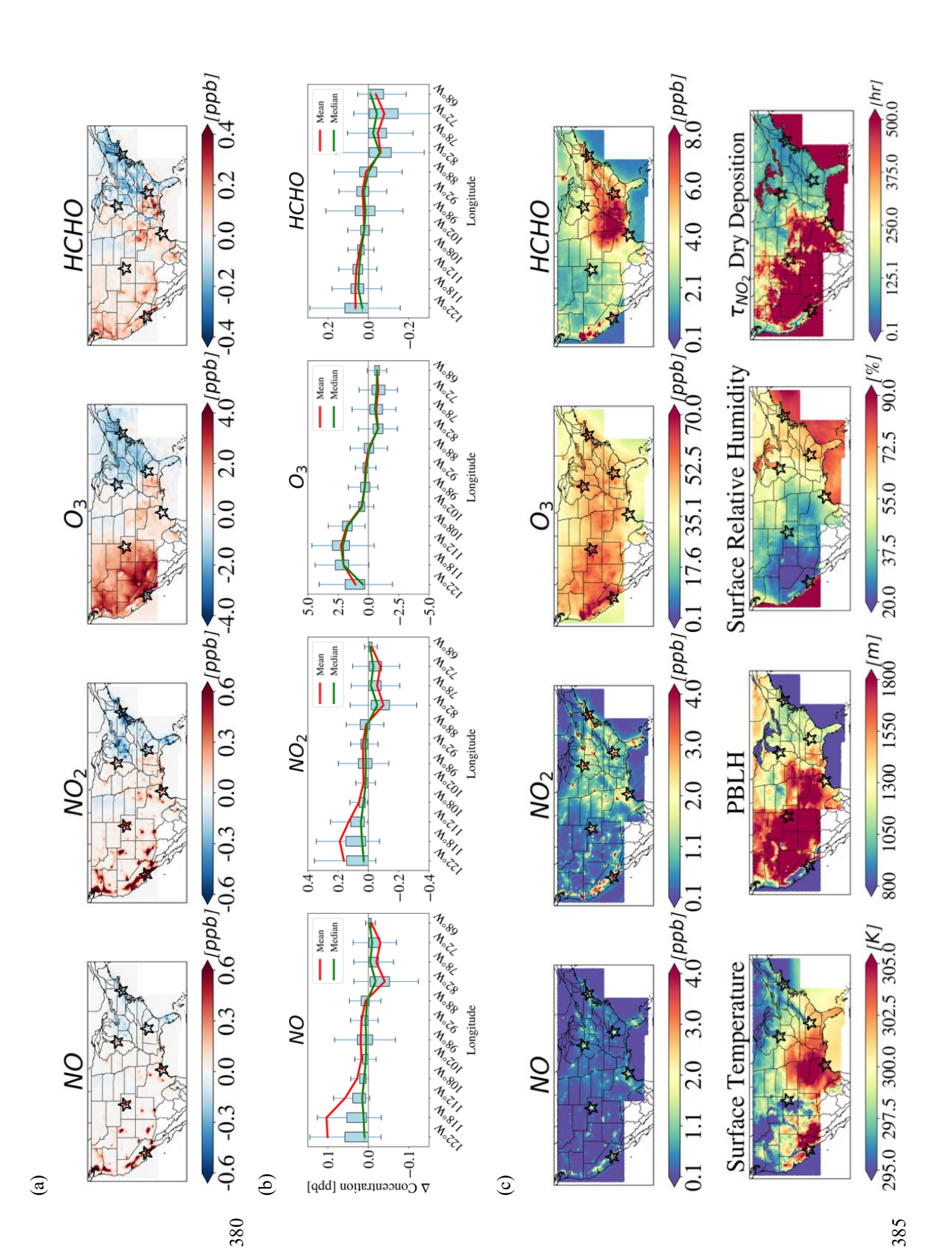


East Coast has higher background NO emissions, approximately 70% higher over the Northeast region than over the West Coast (Fig. 1). The western CONUS displays scattered high-emission hotspots, whereas the eastern CONUS exhibits a more continuous, corridor-like distribution aligned with population density and urban clustering (Fig. S4b). Additionally, biogenic emissions of isoprene and monoterpenes, the dominant biogenic VOC species, are highest in the eastern and southern CONUS (Fig. S5). Switching to hourly emissions generally increases daytime NO (Fig. 6), yet the resulting impact on surface concentrations across the CONUS differs notably from the response to a uniform 30% reduction in anthropogenic NO emissions (Fig. 5). This finding suggests that factors beyond total emissions, such as the timing of emissions perturbations with respect to other processes like meteorology and deposition (discussed below), contribute more to the contrasting changes between the western and eastern CONUS.

This west-east contrast in NO_x and O₃ concentration changes may be driven by differing meteorological conditions across the CONUS (Fig. 5c). In the eastern CONUS, shallower daytime PBLH can limit vertical mixing and enhance both photochemical reactions and surface deposition (Y. Wu et al., 2024). Higher humidity in the eastern CONUS also contributes to shorter O₃ lifetimes (Doherty et al., 2013; Fiore et al., 2002; Racherla and Adams, 2008). Collectively, these processes shorten the NO₂ lifetime against deposition in the eastern CONUS, contributing to greater NO₂ accumulation in the western CONUS.









390

395



Fig. 5: Resolving hourly NO emissions results in contrasting surface responses between the western and eastern CONUS and between urban and rural areas. Panel (a) shows monthly mean July daytime (9 a.m.-5 p.m. local time) differences in simulated surface concentrations of NO, NO₂, O₃, and HCHO (NEI_hourly_NO minus NEI_daily_NO). Panel (b) provides a meridional summary of the July daytime differences shown in panel (a), with values averaged within 5° longitude bins across CONUS latitudes (23-50° N). Each boxplot captures the distribution of differences within each bin (excluding outliers), with red and green lines indicating means and medians, respectively. The horizontal line marks zero change. Panel (c) displays monthly mean July daytime values from the NEI_daily_NO simulation. The first row presents surface concentrations of NO, NO₂, O₃, and HCHO, and the second row includes relevant meteorological variables: surface temperature, planetary boundary layer height (PBLH), and surface relative humidity. The rightmost plot in the second row shows the surface NO₂ lifetime against dry deposition loss. Fig. S9 shows nighttime conditions (11 p.m.-5 a.m. local time), which exhibit changes consistent in direction with those during daytime.





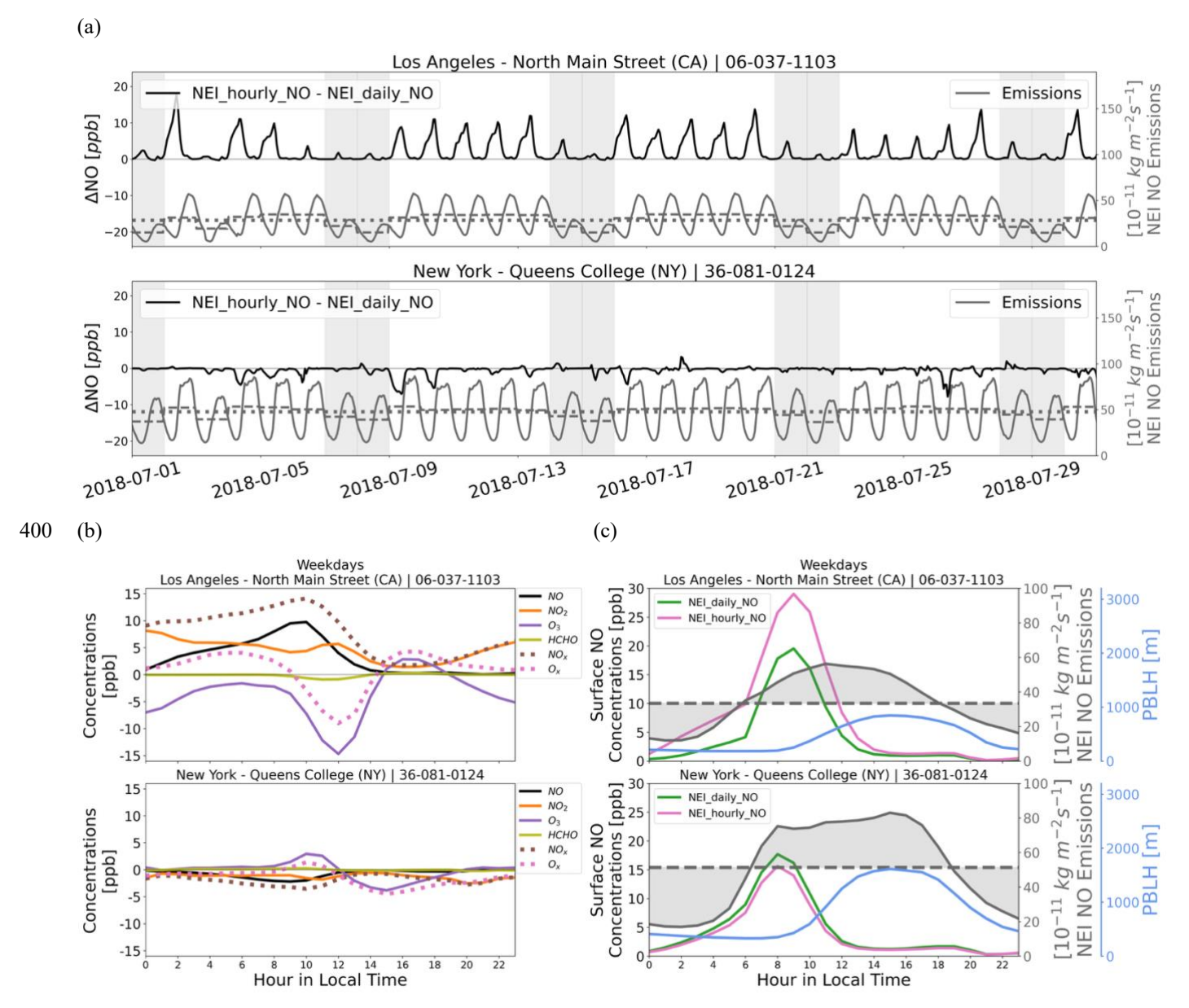


Fig. 6: Despite similar diurnal variation in NO emissions—higher during daytime, lower at night—Los Angeles and New York City show different pollutant responses due to city-specific emission timing, boundary layer dynamics, and local photochemistry. Impact of NO emission temporal resolution (NEI_monthly, NEI_daily_NO, NEI_hourly_NO) on NO emissions and resulting surface concentration responses. (a) Hourly time series of July differences in surface NO concentrations between NEI_hourly_NO and NEI_daily_NO (black solid lines), alongside NO emissions represented as hourly values (solid gray), daily means (dashed), and monthly means (dotted). Weekend days are shaded in gray. July 2018 weekday averages for (b): hourly surface concentration differences between NEI_hourly_NO and NEI_daily_NO for NO (black), NO₂ (orange) O₃ (purple), and HCHO (olive green), with NO₃ (\equiv NO + NO₂; brown) and O₄ (\equiv O₃ + NO₂; pink) shown as dotted lines; (c): hourly NO concentrations from NEI_daily_NO





410 (green) and NEI_hourly_NO (pink), plotted with NO emissions (gray) and planetary boundary layer height (PBLH, blue) for Los Angeles and New York City. Weekend days show similar patterns but with smaller magnitudes of change (Fig. S11). As in panel (a), solid lines represent hourly-varying emissions averaged at each hour over the month, while dashed lines indicate daily-varying emissions averaged similarly. Results for all sites (including Chicago, Denver, Houston, and Atlanta; see Fig. 1), with both weekday and weekend averages shown for panels (b)-(c), are provided in Figs. S10 and S11.

415

420

425

430

435

440

4.1 Urban Case Studies: Los Angeles vs. New York City

To further investigate the regional contrasts introduced in Section 4.1, we examine two representative urban centers: Los Angeles (CA) and New York City (NY). In New York City and Los Angeles, adding hourly variations in NO emissions drives the dominant changes in the simulated diurnal cycle of NO₂ and O₃ concentrations, while variations in other co-emitted species such as CO and anthropogenic VOCs (see Fig. S4) generally have smaller, though occasionally larger, effects (Fig. 4). These case studies illustrate how local-scale meteorology and photochemistry interact with hourly NO emission patterns and result in distinct responses in NO_x and O₃ concentrations. Fig. 6 compares NEI_hourly_NO and NEI_daily_NO simulations, showing (a) time series of NO emissions and surface NO concentration differences, (b) July weekday-averaged diel differences in NO, NO₂, O₃, and HCHO, and (c) weekday-averaged diel cycles of NO emissions, surface NO, and PBLH. Weekend patterns are similar but generally smaller in magnitude (see Fig. S11). Fig. 7 presents July daytime ozone production rates (P(O₃)) binned by surface NO_x concentrations for the NEI_monthly, NEI_hourly_NO, and NEI_monthly_m30anthroNO simulations. Box plots summarize the distribution of P(O₃) within uneven NO_x concentration bins (e.g., 0-1 ppb, 1-2 ppb, ..., 5-10 ppb, 10-15 ppb, ..., >50 ppb), and color-coded points highlight values during morning, noon, and afternoon periods. Results for additional sites (Chicago, Denver, Houston, and Atlanta; see Fig. 1) are provided in Figs. S10-S12.

To assess O₃ production sensitivity to NO_x and VOCs, we apply a 30% uniform, nationwide reduction to monthly mean anthropogenic NO emissions (NEI_monthly_m30anthroNO) and VOC emissions (NEI_monthly_m30anthroVOC), in contrast to the NEI_hourly scenario, where emissions are redistributed across hours without altering total monthly emissions. These MUSICAv0 simulations indicate that urban areas in both the western and eastern CONUS are generally NO_x-saturated, with surface O₃ increasing under reduced NO emissions (Fig. 3). A 30% reduction in anthropogenic VOC emissions yields minimal changes on surface O₃ concentrations (<0.5% across all regions; not shown). Compared to NEI_monthly, reducing anthropogenic NO emissions by 30% (NEI_monthly_m30anthroNO) shifts the distribution and peak of P(O₃) toward lower NO_x levels in both Los Angeles and New York City, suggesting that these urban centers likely remain within a NO_x-saturated regime but are approaching the transition toward NO_x sensitivity (Fig. 7). Previous studies have shown that O₃ production tends to become more NO_x-sensitive around noon and in the afternoon, when photochemical conditions are most favorable for O₃ formation (Mazzuca et al., 2016; Sebol et al., 2024; Tao et al., 2025). In contrast, we find that high P(O₃) values also occur in the late morning in New York City, whereas in Los Angeles they remain more prominent at noon and in the afternoon (Fig. 7).



445

450



Our results suggest that while adding diurnal variations in NO emissions generally redistributes total emissions in a similar way across cities—higher during the day and lower at night (Figs. 6a, 6c)—city-specific features in emission timing and boundary-layer dynamics lead to different concentration responses and distinct shifts in photochemical regimes over the course of the day. Comparing NEI_hourly_NO to NEI_daily_NO, both Los Angeles and New York City show decreases in monthly mean surface O₃, though with different magnitudes and opposite changes in surface NO_x (Fig. 6b). Surface NO_x concentrations increase in Los Angeles, especially during the morning rush-hour with boundary-layer growth, whereas they decrease in New York City. Surface O₃ decreases most in Los Angeles on weekdays between 9 a.m. and 3 p.m., outweighing a smaller late-afternoon increase (3-6 p.m.). In New York City, the net monthly mean decrease is minimal because modest reductions from noon to evening (12-6 p.m.) only slightly exceed the morning increase (8 a.m.-12 p.m.). Incorporating hourly NO emissions (NEI_hourly_NO) reduces July mean daytime O₃ production rates relative to NEI_monthly by ~2 ppb/hr in Los Angeles and ~0.3 ppb/hr in New York City (Fig. 7).

Using hourly NO emissions shifts the distribution and peak of P(O₃) toward higher NO_x concentrations in Los Angeles
and toward slightly lower NO_x in New York City, with more pronounced changes in Los Angeles (Fig. 7). In contrast to the
30% NO reduction case (NEI_monthly_m30anthroNO), the NEI_hourly_NO simulation shifts the P(O₃) distribution in Los
Angeles toward higher NO_x levels, indicating more strongly NO_x-saturated conditions. This suggests that elevated morning
NO_x levels, when the regime is most NO_x-saturated, suppress O₃ formation, and although photochemical conditions still
become more NO_x-sensitive in the afternoon (with rising NO₂ and O₃), the morning reduction dominates the monthly mean O₃
change (Fig. 6b). The more temporally concentrated (peaky) emission profile and shallower daytime PBL heights in Los
Angeles compared to New York City (Fig. 6c), likely amplifies NO_x accumulation, reinforcing a NO_x-saturated regime. Los
Angeles, Denver, and Houston show broadly similar responses, while New York City, Chicago, and Atlanta differ (Figs. S11
and S12).



465

470

475

480



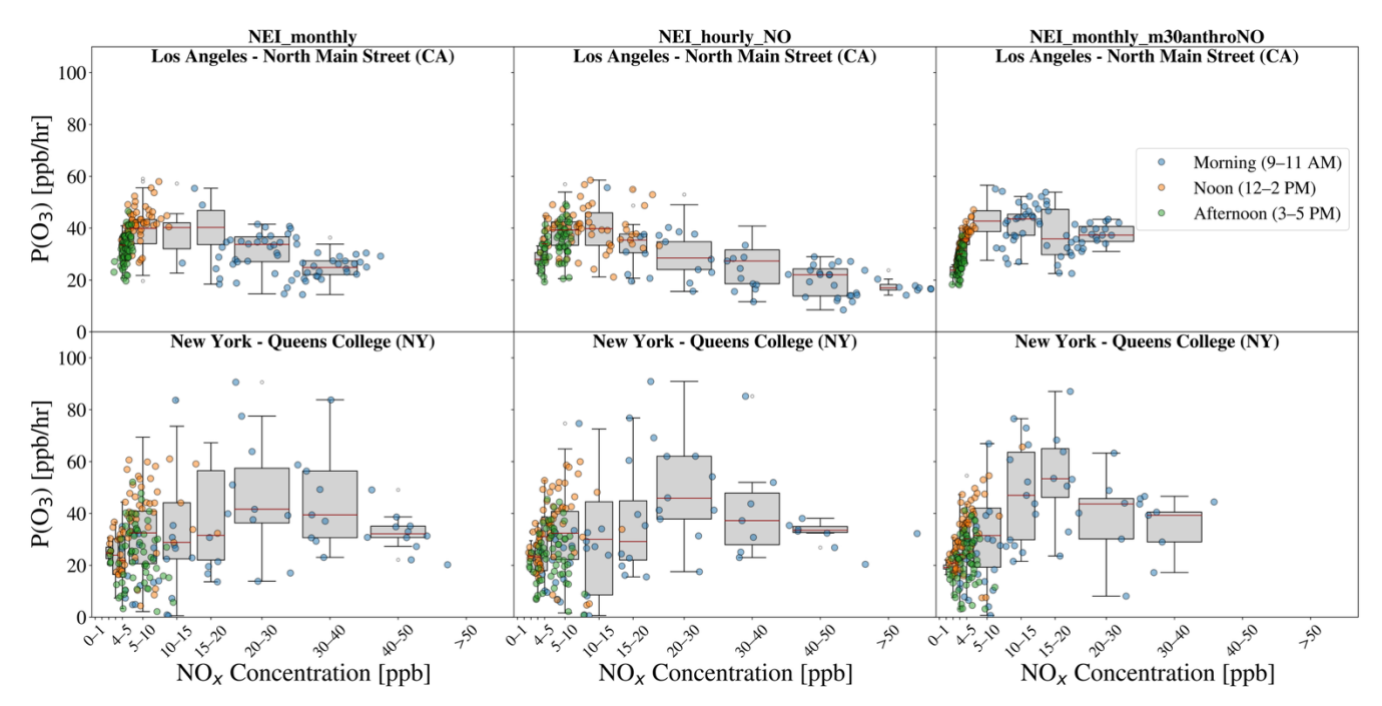


Fig. 7: A uniform 30% reduction in anthropogenic NO emissions shifts the peak $P(O_3)$ distribution toward lower NO_x in both Los Angeles and New York City, whereas resolving hourly NO emissions shifts it toward higher NO_x in Los Angeles but slightly lower NO_x in New York City, suggesting different city-specific impacts on O_3 production chemistry. The figure shows modeled hourly $P(O_3)$ (ppb/hr) versus surface NO_x concentrations (ppb) for July daytime hours (9 a.m.-5 p.m.). Colored points highlight local time windows: morning (9-11 a.m., blue), noon (12-2 p.m., orange), and afternoon (3-5 p.m., green). A boxplot summarizes the distribution of $P(O_3)$ within uneven NO_x bins (e.g., 0-1 ppb, 1-2 ppb, ..., 5-10 ppb, 10-15 ppb, ..., >50 ppb). Only bins containing at least five data points are shown. Box widths roughly reflect the bin ranges, except for the final bin (>50 ppb), which is plotted with a narrower width for visual clarity. Results for additional sites (Chicago, Denver, Houston, and Atlanta; see Fig. 1) are included in Fig. S12.

5 Discussion and Conclusions

Integrating the regional NEI emissions inventory over CONUS into MUSICAv0 improves simulated spatial correlations and reduces biases in surface O_3 and NO_2 concentrations compared to observations (Fig. 2; Table S2). The largest improvements occur in the Northeast, where r_s for O_3 increases from 0.15 to 0.52 and the MBE decreases from +10 ppb (29%) to +4 ppb (13%), and r_s for NO_2 increases from 0.58 to 0.65 and the MBE changes from +4 ppb (61%) to -0.8 ppb (-12%). The model overestimation of surface O_3 decreases in the eastern CONUS when we incorporate hourly varying emissions but worsens in the western CONUS (Fig. 3). Previous studies also find model overestimates of near-surface O_3 , with the most significant biases in the Southeast U.S., possibly reflecting uncertainties in isoprene- NO_x - O_3 chemistry, inaccuracies in dry deposition and forest canopy parameterization, and overestimates in NO_x emissions (Baublitz et al., 2020; Fiore et al., 2009;



485

490

495

500

505

510

515



Makar et al., 2017; Martin et al., 2014; Schwantes et al., 2020b; Travis et al., 2016). We show above that resolving hourly variations in anthropogenic NO emissions also affects simulated O₃ concentrations.

Incorporating hourly NO emissions amplifies the spatial gradients in simulated surface NO₂ concentrations between urban and rural areas, as well as between the eastern and western CONUS, driven by the complex interplay of anthropogenic and biogenic emissions, local photochemical conditions, meteorology, and deposition (Fig. 5). The changes in modeled surface concentrations of O₃ and NO₂ are comparable to, or even exceed, those from a 30% reduction in anthropogenic NO emissions, particularly in some regions of the western CONUS (Fig. 3). Spatial changes in simulated VCD closely follow those in surface concentrations (Fig. 3). In urban areas of both the western and eastern CONUS, resolving hourly NO emissions increases daytime emissions, leading to O₃ decreases of up to 7 ppb in the western CONUS and up to ~2 ppb in the eastern CONUS. In the western CONUS, monthly mean surface NO₂ increases by up to ~6 ppb during the daytime. In contrast, the eastern CONUS with its higher NO and biogenic VOC emissions, larger dry deposition flux rates, more humid conditions, and shallower PBLH—favoring a shorter NO₂ lifetime—experiences daytime NO₂ decreases of up to ~1 ppb. We also find differences in O₃ production regimes across cities: for example, a shift toward more NO_x-saturated conditions in Los Angeles and slightly enhanced NO_x sensitivity in New York City when hourly variations in NO emissions are included.

The sensitivity of monthly mean NO_x concentrations to hourly variations in NO_x emissions highlights the critical importance of accurately accounting for diurnal variations in emissions, particularly since many studies relate or infer emissions from once-daily polar-orbiting satellites (de Foy & Schauer, 2022; Goldberg et al., 2024; Lawal et al., 2022; M. Li et al., 2021; Pu et al., 2022). With the advent of retrievals from the Tropospheric Emissions: Monitoring of Pollution (TEMPO) mission aboard a geostationary satellite launched in 2023, we can now observe trace gases over North America continuously throughout daylight hours (Naeger et al., 2021; Zoogman et al., 2017). Similar geostationary observations have been available since 2020 over the Asia-Pacific region from the Geostationary Environment Monitoring Spectrometer (GEMS), with recent studies demonstrating its capability to capture NO₂ diurnal cycles (Edwards et al., 2024; Park et al., 2025; Yang et al., 2023). Our results demonstrate that hourly variations in emissions can produce nontrivial impacts on NO₂ and O₃ concentrations even without changes in the total emission magnitude. Neglecting such variability may introduce biases when interpreting monthly mean concentrations from once-daily satellite overpasses, potentially aliasing sub-daily emission variability into top-down NO_x emission estimates. Emerging geostationary observations now make it possible to evaluate the intra-day effects directly to refine constraints on emission timing and related photochemical processes.

In summary, we show that incorporating hourly variations in NO emissions produces substantial changes in NO_x and O₃ concentrations, even in monthly average concentrations. These changes, however, are nuanced, differing between urban and rural areas and between the eastern and western U.S., likely reflecting region-specific emission patterns, photochemistry, and meteorological conditions. We showed above that monthly mean surface O₃ over the CONUS in July differs by up to 7 ppb (11% for NEI_hourly relative to NEI_monthly; Fig. 5), large enough to affect model-based conclusions regarding regional attainment of the U.S. National Ambient Air Quality Standards (NAAQS) for O₃.



520

525

540



Although our analysis focuses on July 2018, the differences we identify due to the temporal resolution of emissions are broadly relevant, though their local magnitude will vary across years with both emissions and meteorology. Recent trends since 2018—including continued declines in anthropogenic NO_x emissions (Christiansen et al., 2024), increases in temperature-sensitive soil NO_x and biogenic VOCs (Geddes et al., 2022), more frequent heat waves and stagnation events (Gao et al., 2023), and episodic wildfires (Abatzoglou et al., 2025)—could all modulate the magnitude of these effects. For instance, lower NO_x emissions and flatter diurnal shapes would likely reduce the differences between using hourly and daily or monthly mean emissions, whereas hotter, more stagnant conditions could amplify O₃ sensitivity to the timing of precursor emissions through enhanced photochemical activity. While our study analyzed diurnal emission cycles exclusively within the CONUS during summer, the sensitivities are likely to occur in source regions elsewhere, underscoring the need for further research into diurnal emission cycles and corresponding chemical responses of air pollutants in other seasons and world regions.

Code and Data Availability

The Multi-Scale Infrastructure for Chemistry and Aerosols version 0 (MUSICAv0) is a publicly available community model maintained by the National Center for Atmospheric Research (NCAR). Source code and documentation can be accessed at: https://www2.acom.ucar.edu/sections/MUSICA. Simulation output used in this study has been archived and is available from the corresponding author upon request. Measurements from the State and Local Air Monitoring Stations (SLAMS) network are archived and publicly available through the U.S. Environmental Protection Agency (EPA) Air Quality System Pre-Generated Data Files (U.S. Environmental Protection Agency, 2023). TROPOspheric Monitoring Instrument (TROPOMI)

Level-2 products are available from the NASA Goddard Earth Sciences Data and Information Services Center (GES DISC) for formaldehyde (Copernicus Sentinel-5P, 2018a) and nitrogen dioxide (Copernicus Sentinel-5P, 2018b).

Author contribution

MT set up the model simulations, performed the data analysis, and wrote the manuscript. AMF provided guidance on scientific direction and simulation design, advised throughout the project, and contributed to manuscript revisions. LKE advised on the use of the MUSICAv0 model and provided technical guidance. JRS supported the CESM simulations on high-performance computing (HPC) systems. GGP processed the NEI emissions. DSJ advised on preparing emissions for the variable-resolution grid. WT and the other co-authors provided comments and suggestions to improve the manuscript.

545 Competing Interests

The authors declare that they have no conflict of interest.

Financial Support





This research has been supported by the National Aeronautics and Space Administration (NASA, Health and Air Quality Applied Sciences Team, HAQAST; award no. 80NSSC21K0509) and the National Science Foundation (NSF, award no. 2228379).

References

- Abatzoglou, J. T., Kolden, C. A., Cullen, A. C., Sadegh, M., Williams, E. L., Turco, M., & Jones, M. W. (2025). Climate

 Change Has Increased the Odds of Extreme Regional Forest Fire Years Globally. *Nature Communications*, 16(1),
 6390. https://doi.org/10.1038/s41467-025-61608-1
 - Adams, T. J., Geddes, J. A., and Lind, E. S.: New Insights into the Role of Atmospheric Transport and Mixing on Column and Surface Concentrations of NO₂ at a Coastal Urban Site, Journal of Geophysical Research: Atmospheres, 128, e2022JD038237, https://doi.org/https://doi.org/10.1029/2022JD038237, 2023.
- Baublitz, C. B., Fiore, A. M., Clifton, O. E., Mao, J., Li, J., Correa, G., Westervelt, D. M., Horowitz, L. W., Paulot, F., and Williams, A. P.: Sensitivity of Tropospheric Ozone Over the Southeast USA to Dry Deposition, Geophys Res Lett, 47, e2020GL087158, https://doi.org/https://doi.org/10.1029/2020GL087158, 2020.
 - Christiansen, A., Mickley, L. J., & Hu, L. (2024). Constraining Long-Term NOx Emissions Over the United States and Europe Using Nitrate Wet Deposition Monitoring Networks. *Atmospheric Chemistry and Physics*, 24(7), 4569–4589. https://doi.org/10.5194/acp-24-4569-2024
 - Copernicus Sentinel-5P (processed by ESA): TROPOMI Level 2 Formaldehyde Column Products (RPRO version 02.04.00), European Space Agency [data set], 2018a. https://doi.org/10.5270/S5P-tjlxfd2
 - Copernicus Sentinel-5P (processed by ESA): TROPOMI Level 2 Nitrogen Dioxide Column Products (RPRO version 02.04.00), European Space Agency [data set], 2018b. https://doi.org/10.5270/S5P-s4ljg54
- 570 Crippa, M., Oreggioni, G., Guizzardi, D., Muntean, M., Schaaf, E., Lo Vullo, E., Solazzo, E., Monforti-Ferrario, F., Olivier, J., and Vignati, E.: Fossil CO₂ and GHG Emissions of All World Countries, Publications Office of the European Union, Luxembourg (Luxembourg), https://doi.org/10.2760/687800 (online),10.2760/655913 (print), 2019.
- Danabasoglu, G., Lamarque, J.-F., Bacmeister, J., Bailey, D. A., DuVivier, A. K., Edwards, J., Emmons, L. K., Fasullo, J., Garcia, R., Gettelman, A., Hannay, C., Holland, M. M., Large, W. G., Lauritzen, P. H., Lawrence, D. M., Lenaerts,
 J. T. M., Lindsay, K., Lipscomb, W. H., Mills, M. J., Neale, R., Oleson, K. W., Otto-Bliesner, B., Phillips, A. S., Sacks, W., Tilmes, S., van Kampenhout, L., Vertenstein, M., Bertini, A., Dennis, J., Deser, C., Fischer, C., Fox-Kemper, B., Kay, J. E., Kinnison, D., Kushner, P. J., Larson, V. E., Long, M. C., Mickelson, S., Moore, J. K., Nienhouse, E., Polvani, L., Rasch, P. J., and Strand, W. G.: The Community Earth System Model Version 2 (CESM2), J Adv Model Earth Syst, 12, e2019MS001916, https://doi.org/https://doi.org/10.1029/2019MS001916, 2020.
- Davis, N. A., Callaghan, P., Simpson, I. R., and Tilmes, S.: Specified Dynamics Scheme Impacts on Wave-Mean Flow Dynamics, Convection, and Tracer Transport in CESM2 (WACCM6), Atmos Chem Phys, 22, 197–214, https://doi.org/10.5194/acp-22-197-2022, 2022.



590

610



- Dedoussi, I. C., Eastham, S. D., Monier, E., and Barrett, S. R. H.: Premature Mortality Related to United States Cross-State Air Pollution, Nature, 578, 261–265, https://doi.org/10.1038/s41586-020-1983-8, 2020.
- Di, Q., Wang, Y., Zanobetti, A., Wang, Y., Koutrakis, P., Choirat, C., Dominici, F., and Schwartz, J. D.: Air Pollution and Mortality in the Medicare Population, New England Journal of Medicine, 376, 2513–2522, https://doi.org/10.1056/NEJMoa1702747, 2017a.
 - Di, Q., Dai, L., Wang, Y., Zanobetti, A., Choirat, C., Schwartz, J. D., and Dominici, F.: Association of Short-term Exposure to Air Pollution with Mortality in Older Adults, JAMA, 318, 2446–2456, https://doi.org/10.1001/jama.2017.17923, 2017b.
 - Doherty, R. M., Wild, O., Shindell, D. T., Zeng, G., MacKenzie, I. A., Collins, W. J., Fiore, A. M., Stevenson, D. S., Dentener, F. J., Schultz, M. G., Hess, P., Derwent, R. G., and Keating, T. J.: Impacts of Climate Change on Surface Ozone and Intercontinental Ozone Pollution: A Multi-Model Study, Journal of Geophysical Research: Atmospheres, 118, 3744–3763, https://doi.org/10.1002/jgrd.50266, 2013.
- Edwards, D. P., Martínez-Alonso, S., Jo, D. S., Ortega, I., Emmons, L. K., Orlando, J. J., Worden, H. M., Kim, J., Lee, H., Park, J., and Hong, H.: Quantifying the Diurnal Variation in Atmospheric NO₂ from Geostationary Environment Monitoring Spectrometer (GEMS) Observations, Atmos Chem Phys, 24, 8943–8961, https://doi.org/10.5194/acp-24-8943-2024, 2024.
- Emmons, L. K., Schwantes, R. H., Orlando, J. J., Tyndall, G., Kinnison, D., Lamarque, J. F., Marsh, D., Mills, M. J., Tilmes, S., Bardeen, C., Buchholz, R. R., Conley, A., Gettelman, A., Garcia, R., Simpson, I., Blake, D. R., Meinardi, S., and Pétron, G.: The Chemistry Mechanism in the Community Earth System Model Version 2 (CESM2), J Adv Model Earth Syst, 12, 1–21, https://doi.org/10.1029/2019MS001882, 2020.
- Eskes, H. J., Basart, S., Benedictow, A., Bennouna, Y., Blechschmidt, A.-M., Chabrillat, S., Christophe, Y., Cuevas, E., Flentje, H., Hansen, K. M., Kapsomenakis, J., Langerock, B., Ramonet, M., Richter, A., Schulz, M., Sudarchikova, N., Wagner, A., Warneke, T., and Zerefos, C.: Observation characterisation and validation methods document, Copernicus Atmosphere Monitoring Service (CAMS) report, CAMS84_2018SC2_D6.1.1-2020 observations v5.pdf, https://doi.org/10.24380/7cjp-dn95, 2021.
 - Fiore, A. M., Jacob, D. J., Bey, I., Yantosca, R. M., Field, B. D., Fusco, A. C., and Wilkinson, J. G.: Background Ozone Over the United States in Summer: Origin, Trend, and Contribution to Pollution Episodes, Journal of Geophysical Research Atmospheres, 107, 2002.
 - Fiore, A. M., Dentener, F. J., Wild, O., Cuvelier, C., Schultz, M. G., Hess, P., Textor, C., Schulz, M., Doherty, R. M., Horowitz, L. W., MacKenzie, I. A., Sanderson, M. G., Shindell, D. T., Stevenson, D. S., Szopa, S., Van Dingenen, R., Zeng, G., Atherton, C., Bergmann, D., Bey, I., Carmichael, G., Collins, W. J., Duncan, B. N., Faluvegi, G., Folberth, G., Gauss, M., Gong, S., Hauglustaine, D., Holloway, T., Isaksen, I. S. A., Jacob, D. J., Jonson, J. E., Kaminski, J. W., Keating, T. J., Lupu, A., Marmer, E., Montanaro, V., Park, R. J., Pitari, G., Pringle, K. J., Pyle, J. A., Schroeder, S., Vivanco, M. G., Wind, P., Wojcik, G., Wu, S., and Zuber, A.: Multimodel Estimates of Intercontinental Source-Receptor



625

630

635



- Relationships for Ozone Pollution, Journal of Geophysical Research: Atmospheres, 114, https://doi.org/https://doi.org/10.1029/2008JD010816, 2009.
- Gao, Y., Wu, Y., Guo, X., Kou, W., Zhang, S., Leung, L. R., et al. (2023). More Frequent and Persistent Heatwaves Due To

 Increased Temperature Skewness Projected by a High-Resolution Earth System Model. *Geophysical Research*Letters, 50(18), e2023GL105840. https://doi.org/https://doi.org/10.1029/2023GL105840
 - Gaubert, B., Emmons, L. K., Raeder, K., Tilmes, S., Miyazaki, K., Arellano Jr., A. F., Elguindi, N., Granier, C., Tang, W., Barré, J., Worden, H. M., Buchholz, R. R., Edwards, D. P., Franke, P., Anderson, J. L., Saunois, M., Schroeder, J., Woo, J.-H., Simpson, I. J., Blake, D. R., Meinardi, S., Wennberg, P. O., Crounse, J., Teng, A., Kim, M., Dickerson, R. R., He, H., Ren, X., Pusede, S. E., and Diskin, G. S.: Correcting Model Biases of CO in East Asia: Impact on Oxidant Distributions During Korus-Aq KORUS-AQ, Atmos Chem Phys, 20, 14617–14647, https://doi.org/10.5194/acp-20-14617-2020, 2020.
 - Geddes, J. A., Pusede, S. E., & Wong, A. Y. H. (2022). Changes in the Relative Importance of Biogenic Isoprene and Soil NOx Emissions on Ozone Concentrations in Nonattainment Areas of the United States. *Journal of Geophysical Research: Atmospheres*, 127(13), e2021JD036361. https://doi.org/https://doi.org/https://doi.org/10.1029/2021JD036361
 - Gelaro, R., McCarty, W., Suárez, M. J., Todling, R., Molod, A., Takacs, L., Randles, C. A., Darmenov, A., Bosilovich, M. G., Reichle, R., Wargan, K., Coy, L., Cullather, R., Draper, C., Akella, S., Buchard, V., Conaty, A., da Silva, A. M., Gu, W., Kim, G. K., Koster, R., Lucchesi, R., Merkova, D., Nielsen, J. E., Partyka, G., Pawson, S., Putman, W., Rienecker, M., Schubert, S. D., Sienkiewicz, M., and Zhao, B.: The modern-era retrospective analysis for research and applications, version 2 (MERRA-2), J Clim, 30, 5419–5454, https://doi.org/10.1175/JCLI-D-16-0758.1, 2017.
 - Goto, D., Sato, Y., Yashiro, H., Suzuki, K., Oikawa, E., Kudo, R., Nagao, T. M., and Nakajima, T.: Global Aerosol Simulations Using NICAM.16 on a 14km Grid Spacing for A Climate Study: Improved and Remaining Issues Relative to a Lower-Resolution Model, Geosci Model Dev, 13, 3731–3768, https://doi.org/10.5194/gmd-13-3731-2020, 2020.
 - Granier, C., Lamarque, J. F., Mieville, A., Muller, J. F., Olivier, J., Orlando, J., Peters, J., Petron, G., Tyndall, G., and Wallens, S.: POET, A Database of Surface Emissions of Ozone Precursors, 2005.
 - Guenther, A. B., Jiang, X., Heald, C. L., Sakulyanontvittaya, T., Duhl, T., Emmons, L. K., and Wang, X.: The Model of Emissions of Gases and Aerosols from Nature version 2.1 (MEGAN2.1): an extended and updated framework for modeling biogenic emissions, Geosci Model Dev, 5, 1471–1492, https://doi.org/10.5194/gmd-5-1471-2012, 2012.
- Jo, D. S., Emmons, L. K., Callaghan, P., Tilmes, S., Woo, J.-H., Kim, Y., Kim, J., Granier, C., Soulié, A., Doumbia, T., Darras,
 S., Buchholz, R. R., Simpson, I. J., Blake, D. R., Wisthaler, A., Schroeder, J. R., Fried, A., and Kanaya, Y.:
 Comparison of Urban Air Quality Simulations During the KORUS-AQ Campaign With Regionally Refined Versus
 Global Uniform Grids in the Multi-Scale Infrastructure for Chemistry and Aerosols (MUSICA) Version 0, J Adv
 Model Earth Syst, 15, e2022MS003458, https://doi.org/https://doi.org/10.1029/2022MS003458, 2023.





- Keller, C. A., Long, M. S., Yantosca, R. M., Da Silva, A. M., Pawson, S., and Jacob, D. J.: HEMCO v1.0: A Versatile, ESMF-compliant Component for Calculating Emissions in Atmospheric Models, Geosci Model Dev, 7, 1409–1417, https://doi.org/10.5194/gmd-7-1409-2014, 2014.
 - Kleinman, L. I.: Low and High NO_x Tropospheric Photochemistry, J Geophys Res, 99, 831–838, https://doi.org/10.1029/94jd01028, 1994.
- Kleinman, L. I.: The dependence of tropospheric ozone production rate on ozone precursors, Atmos Environ, 39, 575–586, https://doi.org/10.1016/j.atmosenv.2004.08.047, 2005.
 - Krol, M., Houweling, S., Bregman, B., van den Broek, M., Segers, A., van Velthoven, P., Peters, W., Dentener, F., and Bergamaschi, P.: The Two-Way Nested Global Chemistry-Transport Zoom Model TM5: Algorithm and Applications, Atmos Chem Phys, 5, 417–432, https://doi.org/10.5194/acp-5-417-2005, 2005.
- Lawrence, D. M., Fisher, R. A., Koven, C. D., Oleson, K. W., Swenson, S. C., Bonan, G., Collier, N., Ghimire, B., van Kampenhout, L., Kennedy, D., Kluzek, E., Lawrence, P. J., Li, F., Li, H., Lombardozzi, D., Riley, W. J., Sacks, W. J., Shi, M., Vertenstein, M., Wieder, W. R., Xu, C., Ali, A. A., Badger, A. M., Bisht, G., van den Broeke, M., Brunke, M. A., Burns, S. P., Buzan, J., Clark, M., Craig, A., Dahlin, K., Drewniak, B., Fisher, J. B., Flanner, M., Fox, A. M., Gentine, P., Hoffman, F., Keppel-Aleks, G., Knox, R., Kumar, S., Lenaerts, J., Leung, L. R., Lipscomb, W. H., Lu, Y., Pandey, A., Pelletier, J. D., Perket, J., Randerson, J. T., Ricciuto, D. M., Sanderson, B. M., Slater, A., Subin, Z. M., Tang, J., Thomas, R. Q., Val Martin, M., and Zeng, X.: The Community Land Model Version 5: Description of New Features, Benchmarking, and Impact of Forcing Uncertainty, J Adv Model Earth Syst, 11, 4245–4287, https://doi.org/https://doi.org/10.1029/2018MS001583, 2019.
- Lin, H., Jacob, D. J., Lundgren, E. W., Sulprizio, M. P., Keller, C. A., Fritz, T. M., Eastham, S. D., Emmons, L. K., Campbell, P. C., Baker, B., Saylor, R. D., and Montuoro, R.: Harmonized Emissions Component (HEMCO) 3.0 as a Versatile Emissions Component for Atmospheric Models: Application in the GEOS-Chem, NASA GEOS, WRF-GC, CESM2, NOAA GEFS-Aerosol, and NOAA UFS Models, Geosci Model Dev, 14, 5487–5506, https://doi.org/10.5194/gmd-14-5487-2021, 2021.
 - Makar, P. A., Staebler, R. M., Akingunola, A., Zhang, J., McLinden, C., Kharol, S. K., Pabla, B., Cheung, P., and Zheng, Q.: The Effects of Forest Canopy Shading and Turbulence on Boundary Layer Ozone, Nat Commun, 8, 15243, https://doi.org/10.1038/ncomms15243, 2017.
 - Martin, V. M., Heald, C. L., and Arnold, S. R.: Coupling Dry Deposition to Vegetation Phenology in the Community Earth System Model: Implications for the Simulation of Surface O₃, Geophys Res Lett, 41, 2988–2996, https://doi.org/https://doi.org/10.1002/2014GL059651, 2014.
- Mazzuca, G. M., Ren, X., Loughner, C. P., Estes, M., Crawford, J. H., Pickering, K. E., Weinheimer, A. J., and Dickerson, R. R.: Ozone Production and Its Sensitivity to NO_x and VOCs: Results From the Discover-AQ Field Experiment, Houston 2013, Atmos Chem Phys, 16, 14463–14474, https://doi.org/10.5194/acp-16-14463-2016, 2016.



685

690



- McDuffie, E. E., Smith, S. J., O'Rourke, P., Tibrewal, K., Venkataraman, C., Marais, E. A., Zheng, B., Crippa, M., Brauer, M., and Martin, R. V: A Global Anthropogenic Emission Inventory of Atmospheric Pollutants From Sector- And Fuel-Specific Sources (1970–2017): An Application of The Community Emissions Data System (CEDS), Earth Syst Sci Data, 12, 3413–3442, https://doi.org/10.5194/essd-12-3413-2020, 2020.
- Meinshausen, M., Vogel, E., Nauels, A., Lorbacher, K., Meinshausen, N., Etheridge, D. M., Fraser, P. J., Montzka, S. A., Rayner, P. J., Trudinger, C. M., Krummel, P. B., Beyerle, U., Canadell, J. G., Daniel, J. S., Enting, I. G., Law, R. M., Lunder, C. R., O'Doherty, S., Prinn, R. G., Reimann, S., Rubino, M., Velders, G. J. M., Vollmer, M. K., Wang, R. H. J., and Weiss, R.: Historical Greenhouse Gas Concentrations for Climate Modelling (CMIP6), Geosci Model Dev, 10, 2057–2116, https://doi.org/10.5194/gmd-10-2057-2017, 2017.
- Montzka, S., Aydin, M., Battle, M., Butler, J., Saltzman, E., Hall, B., Clarke, A., Mondeel, D., and Elkins, J.: A 350-Year Atmospheric History for Carbonyl Sulfide Inferred from Antarctic Firn Air and Air Trapped in Ice, J Geophys Res, 109, https://doi.org/10.1029/2004JD004686, 2004.
- Myriokefalitakis, S., Daskalakis, N., Gkouvousis, A., Hilboll, A., van Noije, T., Williams, J. E., Le Sager, P., Huijnen, V.,
 Houweling, S., Bergman, T., Nüß, J. R., Vrekoussis, M., Kanakidou, M., and Krol, M. C.: Description and Evaluation
 of a Detailed Gas-Phase Chemistry Scheme in The TM5-MP Global Chemistry Transport Model (r112), Geosci
 Model Dev, 13, 5507–5548, https://doi.org/10.5194/gmd-13-5507-2020, 2020.
 - Naeger, A. R., Newchurch, M. J., Moore, T., Chance, K., Liu, X., Alexander, S., Murphy, K., and Wang, B.: Revolutionary Air-Pollution Applications from Future Tropospheric Emissions: Monitoring of Pollution (TEMPO) Observations, Bull Am Meteorol Soc, 102, E1735–E1741, https://doi.org/https://doi.org/10.1175/BAMS-D-21-0050.1, 2021.
 - National Center for Atmospheric Research (NCAR): Regridding Meteorological Data, available at: https://github.com/NCAR/IPT/tree/master/Meterological_Reanalysis_Data, last access: 26 January 2022a.
 - National Center for Atmospheric Research (NCAR): Regridding Emissions, available at: https://ncar.github.io/CAM-chem/examples/functions/Regridding.html, last access: 26 January 2022b.
- Park, J., Hong, H., Lee, H., Kim, S.-W., Kim, J., Van Roozendael, M., Fayt, C., Ahn, M.-H., Jacob, D. J., Seo, S., Kim, K.-M., Kim, D., Choi, W., Lee, W.-J., Lee, D.-W., Wagner, T., Richter, A., Krotkov, N. A., Lamsal, L. N., Ko, D. H., Lee, S. H., and Woo, J.-H.: Tropospheric Nitrogen Dioxide Levels Vary Diurnally in Asian Cities, Commun Earth Environ, 6, 389, https://doi.org/10.1038/s43247-025-02272-7, 2025.
- Pfister, G. G., Eastham, S. D., Arellano, A. F., Aumont, B., Barsanti, K. C., Barth, M. C., Conley, A., Davis, N. A., Emmons,
 L. K., Fast, J. D., Fiore, A. M., Gaubert, B., Goldhaber, S., Granier, C., Grell, G. A., Guevara, M., Henze, D. K.,
 Hodzic, A., Liu, X., Marsh, D. R., Orlando, J. J., Plane, J. M. C., Polvani, L. M., Rosenlof, K. H., Steiner, A. L.,
 Jacob, D. J., and Brasseur, G. P.: The multi-scale infrastructure for chemistry and aerosols (MUSICA), Bull Am
 Meteorol Soc, 101, E1743–E1760, https://doi.org/10.1175/BAMS-D-19-0331.1, 2020.
- Racherla, P. N. and Adams, P. J.: The Response of Surface Ozone to Climate Change Over the Eastern United States, Atmos
 Chem Phys, 8, 871–885, https://doi.org/10.5194/acp-8-871-2008, 2008.





- Schwantes, R. H., Emmons, L. K., Orlando, J. J., Barth, M. C., Tyndall, G. S., Hall, S. R., Ullmann, K., St. Clair, J. M., Blake, D. R., Wisthaler, A., and Bui, T. P. V: Comprehensive Isoprene and Terpene Gas-Phase Chemistry Improves Simulated Surface Ozone in the Southeastern US, Atmos Chem Phys, 20, 3739–3776, https://doi.org/10.5194/acp-20-3739-2020, 2020.
- Schwantes, R. H., Lacey, F. G., Tilmes, S., Emmons, L. K., Lauritzen, P. H., Walters, S., Callaghan, P., Zarzycki, C. M., Barth, M. C., Jo, D. S., Bacmeister, J. T., Neale, R. B., Vitt, F., Kluzek, E., Roozitalab, B., Hall, S. R., Ullmann, K., Warneke, C., Peischl, J., Pollack, I. B., Flocke, F., Wolfe, G. M., Hanisco, T. F., Keutsch, F. N., Kaiser, J., Bui, T. P. V, Jimenez, J. L., Campuzano-Jost, P., Apel, E. C., Hornbrook, R. S., Hills, A. J., Yuan, B., and Wisthaler, A.: Evaluating the Impact of Chemical Complexity and Horizontal Resolution on Tropospheric Ozone Over the Conterminous US With a Global Variable Resolution Chemistry Model, J Adv Model Earth Syst, 14, e2021MS002889, https://doi.org/10.1029/2021MS002889, 2022.
 - Sebol, A. E., Canty, T. P., Wolfe, G. M., Hannun, R., Ring, A. M., and Ren, X.: Exploring Ozone Production Sensitivity to NO₂ and VOCs in the New York City Airshed in the Spring and Summers of 2017–2019, Atmos Environ, 324, 120417, https://doi.org/10.1016/j.atmosenv.2024.120417, 2024.
- 730 Sillman, S.: Tropospheric Ozone and Photochemical Smog, Treatise on Geochemistry, 9–9, 407–431, https://doi.org/10.1016/B0-08-043751-6/09053-8, 2003.
 - Sillman, S. and He, D.: Some theoretical results concerning O3-NOx-VOC chemistry and NOx-VOC indicators, Journal of Geophysical Research: Atmospheres, 107, ACH 26-1-ACH 26-15, https://doi.org/https://doi.org/10.1029/2001JD001123, 2002.
- Soulie, A., Granier, C., Darras, S., Zilbermann, N., Doumbia, T., Guevara, M., Jalkanen, J.-P., Keita, S., Liousse, C., Crippa, M., Guizzardi, D., Hoesly, R., and Smith, S.: Global Anthropogenic Emissions (CAMS-GLOB-ANT) for the Copernicus Atmosphere Monitoring Service Simulations of Air Quality Forecasts and Reanalyses, Earth System Science Data Discussions, 2023, 1–45, https://doi.org/10.5194/essd-2023-306, 2023.
- Strosnider, H. M., Chang, H. H., Darrow, L. A., Liu, Y., Vaidyanathan, A., and Strickland, M. J.: Age-specific associations of ozone and fine particulate matter with respiratory emergency department visits in the United States, Am J Respir Crit Care Med, 199, 882–890, https://doi.org/10.1164/rccm.201806-1147OC, 2019.
 - Tang, W., Emmons, L. K., Buchholz, R. R., Wiedinmyer, C., Schwantes, R. H., He, C., Kumar, R., Pfister, G. G., Worden, H. M., Hornbrook, R. S., Apel, E. C., Tilmes, S., Gaubert, B., Martinez-Alonso, S.-E., Lacey, F., Holmes, C. D., Diskin, G. S., Bourgeois, I., Peischl, J., Ryerson, T. B., Hair, J. W., Weinheimer, A. J., Montzka, D. D., Tyndall, G. S., and Campos, T. L.: Effects of Fire Diurnal Variation and Plume Rise on U.S. Air Quality During FIREX-AQ and WE-CAN Based on the Multi-Scale Infrastructure for Chemistry and Aerosols (MUSICAv0), Journal of Geophysical Research: Atmospheres, 127, e2022JD036650, https://doi.org/https://doi.org/10.1029/2022JD036650, 2022.
 - Tang, W., Emmons, L. K., Worden, H. M., Kumar, R., He, C., Gaubert, B., Zheng, Z., Tilmes, S., Buchholz, R. R., Martinez-Alonso, S.-E., Granier, C., Soulie, A., McKain, K., Daube, B. C., Peischl, J., Thompson, C., and Levelt, P.:



755

775



- Application of the Multi-Scale Infrastructure for Chemistry and Aerosols Version 0 (MUSICAV0) for Air Quality Research in Africa, Geosci Model Dev, 16, 6001–6028, https://doi.org/10.5194/gmd-16-6001-2023, 2023a.
 - Tang, W., Pfister, G. G., Kumar, R., Barth, M., Edwards, D. P., Emmons, L. K., and Tilmes, S.: Capturing High-Resolution Air Pollution Features Using the Multi-Scale Infrastructure for Chemistry and Aerosols Version 0 (MUSICAv0) Global Modeling System, Journal of Geophysical Research: Atmospheres, 128, e2022JD038345, https://doi.org/https://doi.org/10.1029/2022JD038345, 2023b.
 - Tang, W., Emmons, L. K., Wiedinmyer, C., Partha, D. B., Huang, Y., He, C., Zhang, J., Barsanti, K. C., Gaubert, B., Jo, D. S., Zhang, J., Buchholz, R., Tilmes, S., Vitt, F., Granier, C., Worden, H. M., and Levelt, P. F.: Disproportionately Large Impacts of Wildland-Urban Interface Fire Emissions on Global Air Quality and Human Health, Sci Adv, 11, eadr2616, https://doi.org/10.1126/sciadv.adr2616, 2025.
- Tao, M., Fiore, A. M., Jin, X., Schiferl, L. D., Commane, R., Judd, L. M., Janz, S., Sullivan, J. T., Miller, P. J., Karambelas, A., Davis, S., Tzortziou, M., Valin, L., Whitehill, A., Civerolo, K., and Tian, Y.: Investigating Changes in Ozone Formation Chemistry during Summertime Pollution Events over the Northeastern United States, Environ Sci Technol, 56, 15312–15327, https://doi.org/10.1021/acs.est.2c02972, 2022.
- Tao, M., Fiore, A. M., Karambelas, A., Miller, P. J., Valin, L. C., Judd, L. M., Tzortziou, M., Whitehill, A., Teora, A., Tian,
 Y., Civerolo, K. L., Tong, D., Ma, S., Adamo, S. B., and Holloway, T.: Insights Into Summertime Surface Ozone Formation From Diurnal Variations in Formaldehyde and Nitrogen Dioxide Along a Transect Through New York City, Journal of Geophysical Research: Atmospheres, 130, e2024JD040922, https://doi.org/10.1029/2024JD040922, 2025.
- Tilmes, S., Hodzic, A., Emmons, L. K., Mills, M. J., Gettelman, A., Kinnison, D. E., Park, M., Lamarque, J.-F., Vitt, F., Shrivastava, M., Campuzano-Jost, P., Jimenez, J. L., and Liu, X.: Climate Forcing and Trends of Organic Aerosols in the Community Earth System Model (CESM2), J Adv Model Earth Syst, 11, 4323–4351, https://doi.org/10.1029/2019MS001827, 2019.
 - Tonnesen, G. S. and Dennis, R. L.: Analysis of Radical Propagation Efficiency to Assess Ozone Sensitivity to Hydrocarbons and NO_x 1. Local Indicators of Instantaneous Odd Oxygen Production Sensitivity, Journal of Geophysical Research Atmospheres, 105, 9213–9225, https://doi.org/10.1029/1999JD900371, 2000.
 - Travis, K. R., Jacob, D. J., Fisher, J. A., Kim, P. S., Marais, E. A., Zhu, L., Yu, K., Miller, C. C., Yantosca, R. M., Sulprizio, M. P., Thompson, A. M., Wennberg, P. O., Crounse, J. D., St. Clair, J. M., Cohen, R. C., Laughner, J. L., Dibb, J. E., Hall, S. R., Ullmann, K., Wolfe, G. M., Pollack, I. B., Peischl, J., Neuman, J. A., and Zhou, X.: Why do Models Overestimate Surface Ozone in the Southeastern United States?, Atmos Chem Phys, 16, 13561–13577, https://doi.org/10.5194/acp-16-13561-2016, 2016.
 - U.S. Environmental Protection Agency (EPA): 2017 National Emissions Inventory (NEI) Data, available at: https://www.epa.gov/air-emissions-inventories/2017-national-emissions-inventory-nei-data, last access: 25 January 2022.



790

800

805

810



- U.S. Environmental Protection Agency (EPA): Air Quality System (AQS) Pre-generated Data Files, available at:

 https://aqs.epa.gov/aqsweb/airdata/download_files.html, last access: August 2023.
 - U.S. Environmental Protection Agency (EPA): Hazardous Air Pollutants, available at: https://www.epa.gov/haps, last access: 23 January 2024.
 - Wang, Y. X., McElroy, M. B., Jacob, D. J., and Yantosca, R. M.: A Nested Grid Formulation for Chemical Transport Over Asia: Applications to CO, Journal of Geophysical Research: Atmospheres, 109, https://doi.org/10.1029/2004JD005237, 2004.
 - Wiedinmyer, C., Kimura, Y., McDonald-Buller, E. C., Emmons, L. K., Buchholz, R. R., Tang, W., Seto, K., Joseph, M. B., Barsanti, K. C., Carlton, A. G., and Yokelson, R.: The Fire Inventory From NCAR Version 2.5: An Updated Global Fire Emissions Model for Climate and Chemistry Applications, EGUsphere, 2023, 1–45, https://doi.org/10.5194/egusphere-2023-124, 2023.
- Williams, J. E., Boersma, K. F., Le Sager, P., and Verstraeten, W. W.: The High-Resolution Version of TM5-MP for Optimized Satellite Retrievals: Description and Validation, Geosci Model Dev, 10, 721–750, https://doi.org/10.5194/gmd-10-721-2017, 2017.
 - Wu, Y., Zhao, K., Ren, X., Dickerson, R. R., Huang, J., Schwab, M. J., Stratton, P. R., Daley, H., Li, D., and Moshary, F.: Ozone Pollution Episodes and PBL Height Variation in the NYC Urban and Coastal Areas During LISTOS 2019, Atmos Environ, 320, 120317, https://doi.org/10.1016/j.atmosenv.2023.120317, 2024.
 - Yang, L. H., Jacob, D. J., Dang, R., Oak, Y. J., Lin, H., Kim, J., Zhai, S., Colombi, N. K., Pendergrass, D. C., Beaudry, E., Shah, V., Feng, X., Yantosca, R. M., Chong, H., Park, J., Lee, H., Lee, W.-J., Kim, S., Kim, E., Travis, K. R., Crawford, J. H., and Liao, H.: Interpreting Gems Geostationary Satellite Observations of the Diurnal Variation of Nitrogen Dioxide (NO₂) Over East Asia, EGUsphere, 2023, 1–25, https://doi.org/10.5194/egusphere-2023-2979, 2023.
 - Yu, K., Jacob, D. J., Fisher, J. A., Kim, P. S., Marais, E. A., Miller, C. C., Travis, K. R., Zhu, L., Yantosca, R. M., Sulprizio, M. P., Cohen, R. C., Dibb, J. E., Fried, A., Mikoviny, T., Ryerson, T. B., Wennberg, P. O., and Wisthaler, A.: Sensitivity to Grid Resolution in the Ability of a Chemical Transport Model to Simulate Observed Oxidant Chemistry Under High-Isoprene Conditions, Atmos Chem Phys, 16, 4369–4378, https://doi.org/10.5194/acp-16-4369-2016, 2016.
 - Zoogman, P., Liu, X., Suleiman, R. M., Pennington, W. F., Flittner, D. E., Al-Saadi, J. A., Hilton, B. B., Nicks, D. K., Newchurch, M. J., Carr, J. L., Janz, S. J., Andraschko, M. R., Arola, A., Baker, B. D., Canova, B. P., Chan Miller, C., Cohen, R. C., Davis, J. E., Dussault, M. E., Edwards, D. P., Fishman, J., Ghulam, A., González Abad, G., Grutter, M., Herman, J. R., Houck, J., Jacob, D. J., Joiner, J., Kerridge, B. J., Kim, J., Krotkov, N. A., Lamsal, L., Li, C., Lindfors, A., Martin, R. V, McElroy, C. T., McLinden, C., Natraj, V., Neil, D. O., Nowlan, C. R., O'Sullivan, E. J., Palmer, P. I., Pierce, R. B., Pippin, M. R., Saiz-Lopez, A., Spurr, R. J. D., Szykman, J. J., Torres, O., Veefkind, J. P.,





Veihelmann, B., Wang, H., Wang, J., and Chance, K.: Tropospheric emissions: Monitoring of pollution (TEMPO), J Quant Spectrosc Radiat Transf, 186, 17–39, https://doi.org/https://doi.org/10.1016/j.jqsrt.2016.05.008, 2017.